Viability Assessment of Enhancing Dry Cooling Systems using Thermal Storage Ponds

By:

Priyesh Gosai

Thesis presented in fulfilment of the requirements for the degree of Master of Science in Engineering in the Faculty of Engineering and the Built Environment at The University of Cape Town

Supervisor: A/Prof. A. G. Malan

Co-supervisor: Dr. J.P. Pretorius

June 2014

Declaration

By submitting this, I declare that the entirety of the work contained therein is my own, original work, that I am the authorship owner thereof (unless to the extent explicitly otherwise stated) and that I have not previously in its entirety or in part submitted it for obtaining any qualification.

Date: 20/05/2014

Signed by candidate

Abstract

Dry cooled systems are employed to reject heat in modern power plants. Unfortunately, these cooling systems become less effective under windy conditions and when ambient temperatures are high. One proposed solution to this problem is to augment the cooling capacity of the dry cooled system by means of utilizing evaporative cooling ponds which can be operated in parallel during adverse ambient conditions. This study investigates a concept for a South African power station. The system utilises waste-water from evaporation ponds which will supply a surface condenser connected in parallel to the dry cooled system. The development of this system requires an accurate model to predict the transient thermal response of the pond. No such pond model is available in open literature due to the pond under consideration having a unique size as well as size to depth ratio. Various heat transfer modes are numerically modelled for large evaporation ponds, including free surface evaporation which is a transient and complex phenomenon. Evaporation at the surface is the primary heat and only mass transfer driver. The modified Ryan equation proposed by an experimentally validated study was used to estimate evaporation on the surface. Convection is modelled using a correlation that was derived and experimentally tested for applications in the natural environment. Heat transfer via conduction to the ground is solved using a one dimensional finite difference solution to the heat conduction equation, and radiation is modelled using widely accepted correlations. These correlations were coupled and implemented into a computer model using C++. Through numerical analysis the relevance and accuracy of each transfer mode was rigorously analysed. Once validated, the intended loading conditions at the power station were imposed onto the pond model in order to assess its cooling viability. It is concluded that the pond not only poses a sustainable and environmentally neutral cooling augmentation device, but is also cost effective.

Acknowledgments

Jai Shri Krishna,

This thesis could not be possible without the support from my sponsors and numerous individuals who have been a positive influence in my studies.

- Prof. Arnaud Malan, thank you for the expert advice and involvement in the work for this thesis.
- Dr Johannes Pretorius and Dr Francois du Preez, thank you for your expert advice in this research and your leadership during my training that lead me towards my post-graduate studies.
- Hein Goldschagg, ACC Engineer at Matimba Power Station, thank you for motivating this project and having me part of the team investigating this system.
- My parents, Arwin and Madhuri Gosai, thank you for the encouragement and support you have always given to me.
- The group of students from the Nuclear Mezzanine in the Department of Mechanical Engineering, thank you for being superb office mates. A special thanks to Andrew Mowat and Nathan Zhouen for helping me through the low points of debugging C++ code.
- Last but not least I would like to thank the management of Eskom for the development of the Eskom Power Plant Engineering Institute. It is an ambitious and progressive initiative which is developing technical competencies the South African Power Industry.

Contents

List of Figures

List of Tables

Nomenclature

Symbols

β	Thermal expansion coefficient $\frac{m^3}{m^3}$
ϵ	Emissivity
μ'	Extinction coefficient
μ	Dynamic viscosity N/sm
ν	Kinematic viscosity $\frac{m^2}{s}$
ω	Humidity ratio
$\overline{q}$	Surface heat flux W/m^2
$\overline{R}$	Bowen ratio
Φ_{rh}	Relative humidity
ρ'	Reflectance %
ρ	Density kg/m^3
σ	Stephan-Boltzman constant $\frac{J}{m^2sK^4}$
τ	Transmittance %
θ	Virtual temperature K
θ_r	Angle of incidence $^\circ$
A	Pond surface area m^2
a	Coefficient representing the proportional convection via evaporation kg/m^2

b	Coefficient representing the proportional forced convection via evaporation kg/m^2
C	Molar concentration of the species $kmol/m^3$
c	Vapour Concentration kg/m^2
C_f	Skin friction coefficient
c_p	Specific Heat Capacity $J/kg.K$
$const$	arbitrary constant for free convection from a thermal boundary layer
D	Binary diffusion coefficient m^2/s
d	arbitrary constant for forced convection from a thermal boundary layer
E	Energy W
e	Vapour Pressure Pa
g	Gravitational acceleration m/s^2
I_b	Solar beam radiation $\frac{W}{m^2}$
I_d	Solar diffuse radiation $\frac{W}{m^2}$
k	Thermal conductivity W/mK
L	Length along pond surface m
L_v	Latent heat of vapourisation J/kg
N''	Molar flux of species $kmol/s.m^2$
P	Pressure Pa
Q	Heat/Energy J
q	Heat transfer flux rate W/m^2
r	Un-polarised solar radiation coefficient
R_v	Universal gas constant $\frac{J}{K.mol}$
T	Temperature K or $^\circ C$

t	time s
V	Volume m^3
v	velocity $\frac{m}{s}$
x	Direction vector along the pond surface
y	Direction vector normal to pond surface

Subscripts

∞	Free stream condition
$\parallel$	Parallel
$\perp$	Perpendicular
a	Atmospheric
atm	Atmospheric
av	Air vapour mixture
$cond$	Conduction
$conv$	Convection
dp	Dew Point
$evap$	Evaporation
$film$	Average conditions
$fluid$	Fluid Flow
$precip$	Precipitation
rad	Ground Water
s	Surface
sky	Sky condition
sol	Solar

st	Stored
$stored$	Retained within control volume
$vapour$	Vapour
$vapour - water$	Vapour water mixture
$water$	water
abs	Absolute
air	air property
v	Saturated vapour

Superscripts

n	Exponential coefficient
$t1$	Quantity based on the conditions at the beginning of a time step
$t2$	Quantity based on the conditions at the end of a time step
tot	Total

Abbreviations

ACC	Air Cooled Condenser
agl	Above Ground Level
CFD	Computational Fluid Dynamics
ECP	Evaporative Cooling Pond
EPPEI	Eskom Power Plant Engineering Institute
EPRI	Electric Power Research Institute
HVAC	Heating, Ventilation and Air-Conditioning
LP	Low Pressure
ppm	parts per million

SOC	State owned company

Dimensionless Parameters

Nu	Nussult Number $\frac{hL}{k}$
Pr	Prandtl number $\frac{c_p \mu}{k}$
Ra	Rayleigh's Number $\frac{g\beta(\Delta T)x^3}{\nu k}$
Sc	Schmidt Number $\frac{\mu}{\rho d}$

Chapter 1

Introduction

1.1 Background

The large coal reserves in South Africa has resulted in the installation of coal fired power plants as a primary source of energy. The shortage of generating capacity currently being experienced has however forced the local utility to operate on a thin reserve margin. Therefore inefficiencies which affect these plants need to be addressed in order to meet power demands. In addition, rapid global climate change is a serious concern. The improvement of plant efficiency and the reduction in environmental impact are therefore key considerations for the power industry.

An ambitious project in the late 1980's saw the construction of Matimba Power Station shown in Figure 1.1. The station is made up of six units each capable of generating 665MW of gross electrical energy. Matimba Power Station is located in South Africa's coal rich Lephalale region. The area is semi arid and water is scarce. This required the use of a direct dry cooling system also called an Air Cooled Condenser (ACC). When constructed, Matimba Power Station was 11 times larger than any other dry cooled power plant in the world. The ACC at Matimba Power Station is made up of elliptic fin tube bundles arranged in an A-formation. These structures are placed on $45m$ high concrete columns located against the Turbine Hall as shown in Figure 1.1. Electrically driven fans below the bundles force the flow of air over the elliptic fin tubes. Louw [9] describes the orientation of the plant to favour

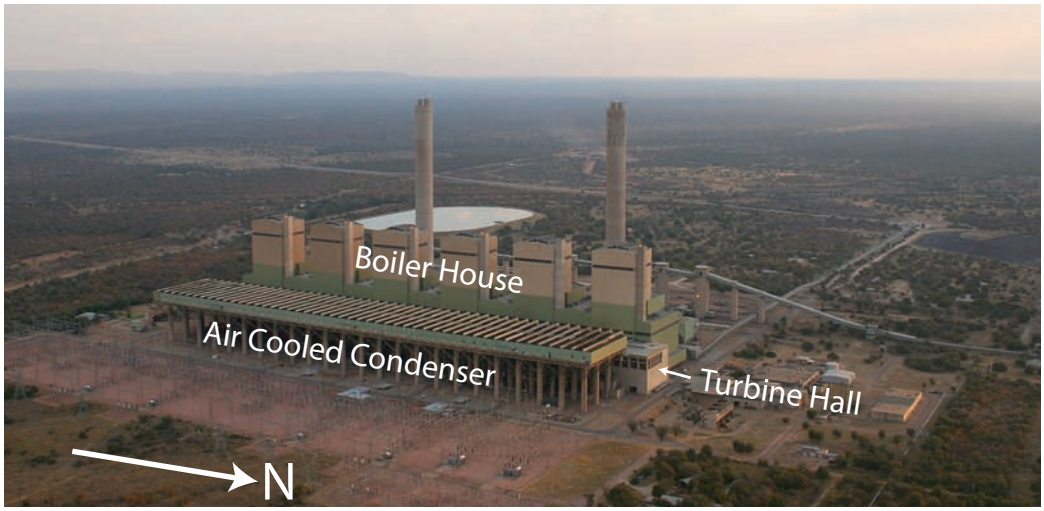

Figure 1.1: Matimba Power Station seen from the East with the A-Frame ACC units in the foreground

dominant easterly winds to assist cooling. The result of this orientation however leaves the station under threat by less frequent westerly winds which reduce the air flow into the ACC, when coupled with problems associated to the high ambient temperatures the losses incurred are significant.

The heat rejected by an ACC is directly linked to the atmospheric dry bulb temperature and the mass flow rate of air passing through its massive heat exchanger bundles. During periods where high ambient temperatures in Lephalale and the undesirable flow patterns induced by westerly winds are experienced, the cooling capacity of the ACC is significantly diminished. This results in the condenser operating at a far higher pressure which decreases the efficiency of the steam turbine system. In these conditions the high condensing pressure must be moderated by reducing the unit output and this phenomenon is termed "Vacuum Load Losses" [2]. As Matimba Power Station is currently in the middle of its fifty year design life, improvements made to the plant will result in significant benefits over the remaining operating time. Solutions to address Vacuum Load Losses are therefore being considered.

In light of the above, the experience gained by the operators have resulted

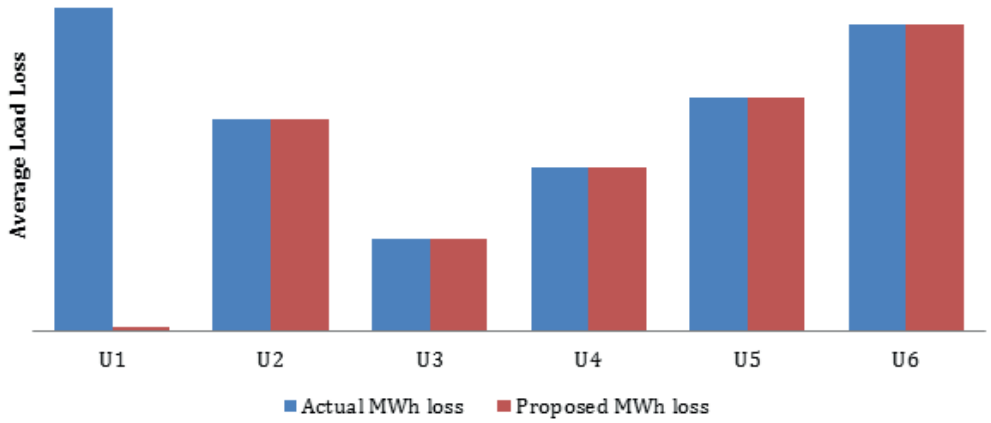

Figure 1.2: Losses currently experienced on each unit at Matimba Power Station and the proposed reduction in losses as a result of the ECP system [2]

in numerous studies intended to improve the plant's performance. Goldschagg [10] describes the experience during the first five years of operation. This experience together with a long standing research initiative at the University of Stellenbosch, has resulted in numerous advances that have improved the operation of the ACC's. Modifications made to the boiler house have improved the distribution of air to the ACC during westerly winds. The inclusion of walkways and wind-walls on the outer perimeter have further reduced losses as a result of hot air recirculation. While these changes have been implemented, incidents can still occur where up to $350MW$ is lost on a single unit. Losses are most prevalent on the outer units as shown in Figure 1.2. Where losses occur at peak demand periods the utility would need to meet the gap in power on the national grid through the use of peaking plants which are very expensive to operate.

Due to the above, the utility has launched numerous studies into reducing Vacuum Load Losses incurred at Matimba Power Station. The concept investigated in this study considers the use of waste water ponds situated at the plant have the potential to capture heat from the plant during adverse conditions and naturally reject heat to the environment. These evaporation ponds (each with $45,000m^2$ surface area) capture plant waste water which cannot

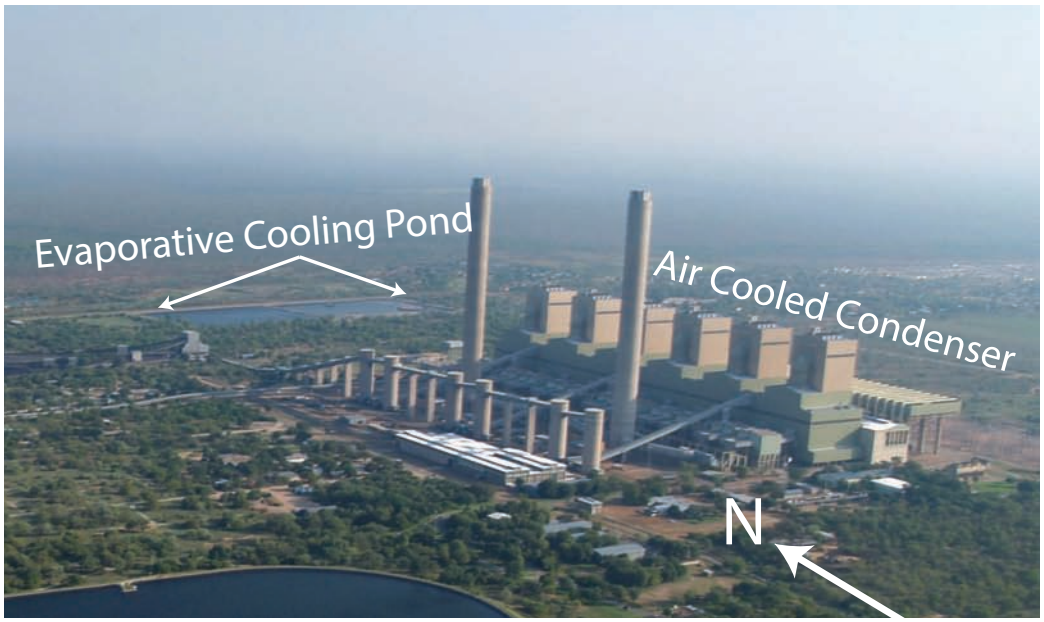

Figure 1.3: Matimba Power Station seen from the South-West. The Evaporative cooling pond is seen North of the station

be discharged into the local environment due to the chemical composition (see Figure 1.3 and Table 1.1).

The operation of this system is proposed by Goldschagg [2], who considers the possibility of water leaving the condenser being added to the evaporation pond and left to cool naturally. This would alter the function of the pond to that of an Evaporative Cooling Pond (ECP). Assessing the thermal viability of the ECP is the objective of this study.

The ECP cooling system configuration under consideration is schematically shown in Figure 1.4. During adverse atmospheric conditions described above, the majority of steam leaving the power plant's low pressure turbine (LP turbine) will be condensed in the ACC. However the augmentation will allow for a portion of the steam to instead pass through the surface condenser. Cooling water drawn from the ECP is supplied to the surface condenser and will absorb heat from steam entering the condenser after which the heated water will return to the pond. The effect of this heat exchange will result in steam condensing before being pumped to the condensate tank mixing with water condensed in the ACC. This system will operate intermittently depending on the risk of a Vacuum Load Loss incident and the availability

Table 1.1: Typical Chemical Profile of Water in Evaporation Ponds

Parameter	**Measurement**
Turbidity(NTU)	2.89
pH	4.23
$K_{25}(\mu S/cm)$	1346
Calcium Hardness (ppm as $CaCO_3$)	352.1
Total Hardness (ppm as $CaCO_3$)	352.1
Silica (SiO_2 ppm)	20.07
Suspended Solids(ppm)	121
Chlorine(ppm)	0.1

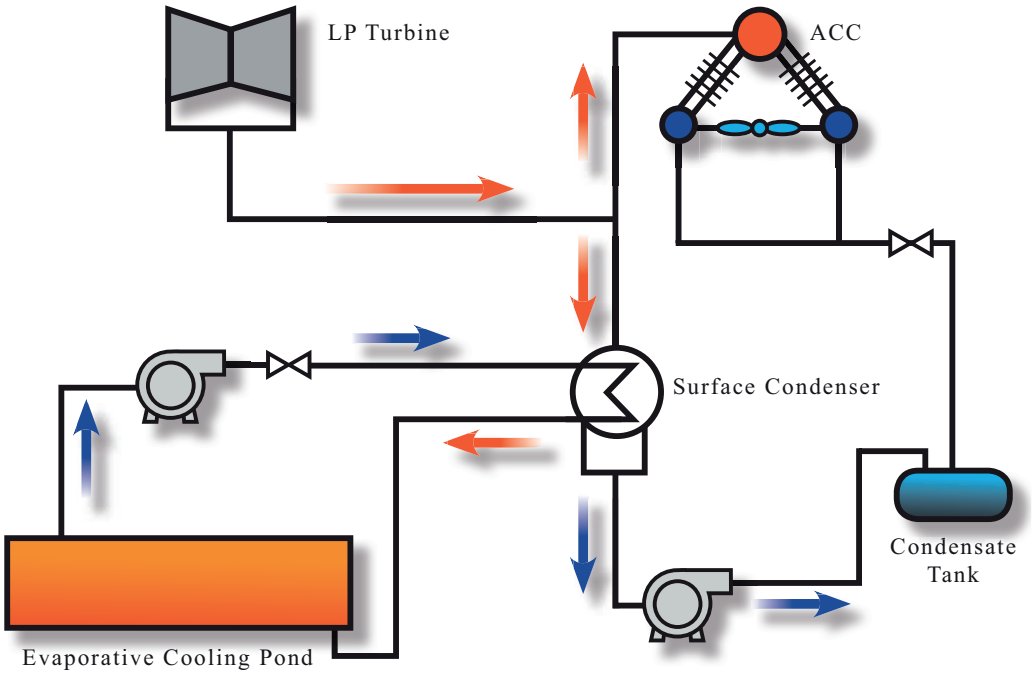

Figure 1.4: Cooling pond concept

of cold water in the pond. The hot water returning to the pond will be left to cool.

The use of ECPs in the power generation industry dates back to the 1900's. As power output increased it was replaced with active cooling systems such as cooling towers. A key influential factor to the use of the ECP as described is its ability to adequately reject heat to the natural environment. In this regard two crucial parameters which determine the viability of the cooling pond as a sustainable solution need to be quantified, viz. the time it would take for the pond to return to its original temperature and the water lost through evaporation from the pond as a result of the added heat. However, a mathematical model that describes the associated diurnal thermal response of an ECP of this size does not exist in the open literature. Such a model is therefore to be developed, which is the focus of this project.

1.2 Scope of Work and Research Contributions

As outlined above, the ECP system will serve the purpose of adding additional cooling during adverse conditions. Therefore, the system will operate for short periods of time (circa two hours), once conditions improve and the need for the cooling system is eliminated, and the ECP system will be shut down. It is also anticipated that the cooling water outlet and hot water inlet will be placed at opposite ends of the pond such as to avoid short-circuiting of hot water. During operation the general flow of water into and out of the pond will result in a certain pond thermal profile. Once the system is stopped, the mixing of warm and cold water would be a result of the natural dynamic processes to influence flow in the pond. The excess heat in the pond would then be dissipated from the pond to the natural environment.

The rate of this heat dissipation needs to be such that, should the ECP system be required for several hours on a daily basis, two conditions are met: the temperature of water being supplied to the condenser should be such that cooling water is always available and at a temperature which is close to a sufficiently low temperature to optimise condenser performance; and evaporation of cooling water is such that the pond does not dry out. This study is to develop a mathematical model that would allow answering these

particular questions with a high degree of certainty.

Existing pond models in open literature are developed for specific applications. The areas of interest from these studies are assessed with great depth in the applicable subject. Hamblin and Imberger [11] describes the effects of forces applied to lakes, by the surrounding environment, on the motion of fluid within the water body and heat exchange. Models which describe these dynamics can be investigated at various scales. The mean motion within a pond is dependent on its shape, size and location when compared to the magnitude of the thermo-fluid force applied. Stratification within a water body is a result of the natural retardation of vertical flows [12]. Such features change the thermal characteristics of the water body, with an example being the stratification experienced in solar ponds. High salinity water bodies form distinct thermal convective layers. The natural boundary developed by these layers are utilised to store solar energy which may be extracted for energy generation applications [13]. Water bodies with continuous in and out flows develop profiles based on the conditions of water entering and its density compared to the water in the pond [11].

The generalised structure of a water body has been categorised for application to specific models. Jirka and Harleman [14] presents a dimensionless parameter called the pond number, valid for ponds with continuous flow. The potential heat capacity, degree of mixing and the resulting internal fluid structure which will be developed is indicated by this number. Kirillin [12] summarises other parameters characterising pond structure. The ECP at Matimba Power Station will have no active flow for a majority of its life. Therefore such parameters do not adequately describe this pond.

The dynamics described by Kirillin [12] indicate that the internal flow patterns will favour an increased surface temperature. Convective heat exchange is increased in such instances. The conservative assumption may therefore be made that the pond temperature is uniform. This provides a conservative estimate on the heat rejection rate since convection would on the other hand drive warmer water to the water surface increasing its heat transfer rate with the environment. Thermal models developed for the power industry are given by Raphael [15]. The model assumes uniform vertical temperature distributions and predicts changes in a river being used as a heat sink. Jobson [16] also developed a mathematical model for the prediction of a pond performance. The work was aimed at the rejection of excess heat from water systems through the use of large water bodies. The same approach was followed by Olwi et. al. [17] for passive cooling systems which used ponds as

heat sinks in desert environments. In the interest of water conservation the ponds were covered using white aluminium sheets. Lumped thermal models often appear in literature in HVAC applications such as Chiasson [18].

The type of modelling techniques used to simulate cooling ponds is typically based on the available resources and the scale of the application. Numerical discretisation techniques employed by Bachu et.al. [19] used an implicit finite difference scheme to solve a one dimensional heat balance on a solar pond. Such work has been advanced using modern tools in similar studies [13]. Here Computational Fluid Dynamics (CFD) was used to predict surface heat exchange in solar ponds. Models developed for natural lakes, which predict the dynamics of ecological processes [20] also use CFD. When however considering the particularly large specific area (which is exposed to complex and fluctuating wind flow patterns) of the pond under consideration, CFD would be expensive and was therefore deemed premature at this point. A lumped thermal model is not only simpler, but similar to Codell et.al. [21], may be employed to calculate an upper and lower operational bound for the pond. Viability estimates may then be extracted from the latter. Therefore it is decided that a lumped thermal pond model is developed for the intended application.

Studies where the performance of ECPs via lumped thermal approaches are modelled were identified. A significant study conducted circa 1980 investigated the development of equations which predict water losses from cooling ponds. This study by Adams et.al. [4] evaluated numerous equations that predict evaporation from a heated body of water.

The heat and mass transfer modes affecting the pond at Matimba Power Station are shown in Table 1.2. Evaporation is expected to be a dominant heat exchange mode. Thermal convection and thermal radiation are expected to be smaller in magnitude however significant. The complex nature of the data required to measure solar heat addition implies that the inclusion of heat from this mode should be conducted with caution. Therefore this study will investigate the relevance of solar radiation to the pond and appropriately include this into the pond model. Addition of water through precipitation and over-land run-off inherently accelerate the cooling process and exclusion of these heat exchange modes would provide a conservative result. The mixing of water within the pond is a complex process and for the intended viability study the pond surface will initially be assumed uniform. Thereafter the accuracy of the model can be improved through the analysis of the actual flow within the pond. The effect of ground conduction compared to

Table 1.2: Factors influencing the pond

Region	**Factor**
Surface	Evaporation
	Thermal Convection
	Thermal Radiation
	Solar Radiation
	Over-Land Run-off
	Precipitation
Internal	Mixing
	Water in/out flows
Ground	Conduction
	Seepage

other heat exchange mechanisms is expected to be small in magnitude. The study will quantify this difference and investigate factors influencing ground conduction. Lastly, the rubberised canvas covering the pond floor will not allow for any seepage, therefore no water is lost through seepage.

Using the theory of a thermodynamic control volume described by Bergman et.al. [22], Equation (1.1) is incorporated for the development of a transient thermal pond model.

$$\Delta E_{st}^{tot} = \Sigma q \tag{1.1}$$

where ΔE_{st}^{tot} is the net change in energy within the control volume and q represents the numerous heat exchange modes affecting the pond. The heat exchange modes relevant to the pond (shown in Figure 1.5) are then included in this study and the final governing equation for the transient thermal pond model is given by Equation (1.2).

$$\frac{dT}{dt} V \rho c_p = q_{evap} + q_{conv} + q_{rad} + q_{sol} + q_{ground} + q_{flow} \tag{1.2}$$

The resulting model using Equation (1.2) would be capable to provide design information for the ECP system. The operating constraints which define the periods for which the pond may be used and the associated water loss are

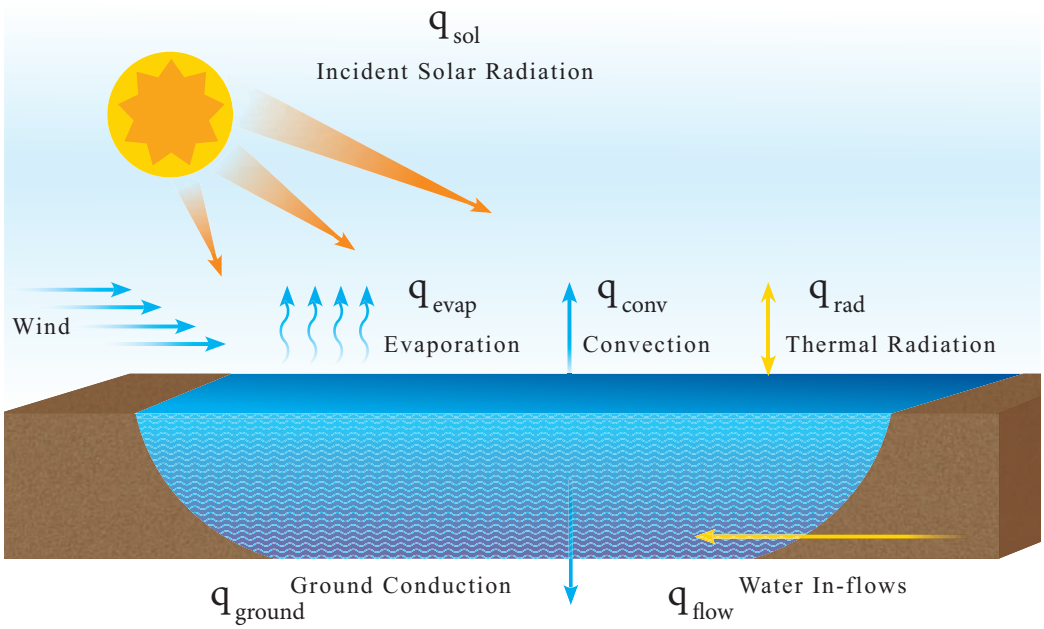

Figure 1.5: Modes of heat transfer evaluated in this model

of primary concern. The rate at which the pond would cool will determine whether or not the system would be practical for implementation. Once these factors are known, the influential atmospheric parameters can be established and the optimisation of the operating parameters for the cooling pond established.

1.3 Project Plan

The transient thermal model for the ECP at Matimba Power Station is developed in the chapters to follow. A detailed study is conducted into the heat transfer modes which affect the cooling pond. These are then implemented into a suitable computer model to allow for the simulation of the cooling pond operation.

This thesis is structured into five chapters, with the contents of the remaining four chapters being:

- Chapter 2: Pond Thermal Model

  In chapter one, the review of pond models in literature reveals that each heat transfer mechanism needs to be carefully investigated. The effect of these mechanisms is investigated through individual literature studies in Chapter 2. The outcome of these studies will generate correlations which are validated using a mixture of experimental data and mathematical analysis. The results are implemented into the final model described in Chapter 3.

- Chapter 3: Numerical Model

  In this chapter the development of a numerical model to predict the hydrodynamic performance of a cooling pond is described. The chapter is completed by a validation of the complete model using experimental results.

- Chapter 4: ECP Viability Study

  The final model is now utilised for the generation of results that will provide quantitative data. Such data can be used to predict the pond operational bounds, which will enable assessing the viability of the ECP to eliminate the losses experienced on a single unit at Matimba Power Station.

- Chapter 5 Conclusions

  This chapter concludes the study. The process of gathering relevant correlations and validating this model has resulted in the development of a numerical model. This model predicts the diurnal variation in pond temperature and the assessment of the final results is presented.

Chapter 2

Pond Thermal Model

The various ECP heat transfer modes referred to by the terms in Equation (1.2) are now individually investigated viz. evaporation, convection, radiation and conduction. A study of the literature in conjunction with taking cognisance of the data available from Matimba Power Station will inform the selection of appropriate correlations.

2.1 Evaporation

Evaporation constitutes the vaporisation of a liquid into a gaseous phase which is not saturated with the evaporating substance. Sartori [23] states that nearly 50% of the heat exchanged is as a result of evaporation from a free water surface. Further bearing in mind the large surface area of the pond under consideration, evaporation is expected to be the dominant heat transfer mechanism in this study. The functional relevance of evaporation to the performance of the plant is shown in Figure 2.1. Once heated, the ECP water temperature will invariably approach the atmospheric wet-bulb temperature. In addition the water lost would require replenishment while effecting the chemistry of the pond. Therefore, a quantitative understanding of the heat and mass exchanges which occur as a result of evaporation is of primary importance for this study.

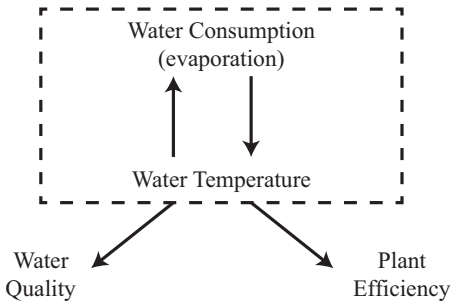

Figure 2.1: Functional Relationship for Pond Performance [3]

2.1.1 Literature Study

Flow over water surfaces will result in the formation of boundary layers, of which three are described by Bergman et.al. [22] (see Figure 2.2). Firstly the velocity boundary layer (A) is coupled to the no slip condition assumed at the surface of the pond. This will generate a velocity profile (B) approaching the free stream speed as one moves away from the pond surface. Secondly the thermal boundary layer (D) is developed as a result of the variation in temperature (shown by (C)) between the water surface and the air stream. This boundary layer will affect the rate of heat transfer by convection and will be discussed in further detail in Section 2.2. The variation in vapour concentration (C_{vapour}) normal to the pond surface (E) approaching the air stream will develop a concentration boundary layer (F). The magnitude of this concentration difference will influence the vapour molar flux rate (N''_{vapour}) at the surface. The binary diffusion coefficient ($D_{vapour-water}$) is the constant of proportionality used to obtain the magnitude of the molar flux rate, in the absence of air movement, referred to as Fick's law [22].

$$N''_{vapour} = -D_{vapour-water}\frac{\partial C_{vapour}}{\partial y} \tag{2.1}$$

where y is the direction vector normal to the pond surface. In the case of the ECP, evaporation is strongly effected by the advection of water vapour via flow. The structure of the flow field above the pond is therefore divided into four distinct regimes (shown in Figure 2.3). The flow structure is dependent on the intensity of the wind passing the water surface and the pond thermal state. The first regime is termed free convection, which is prevalent in the absence of wind. Here, flow is directed normal to the pond surface (as depicted

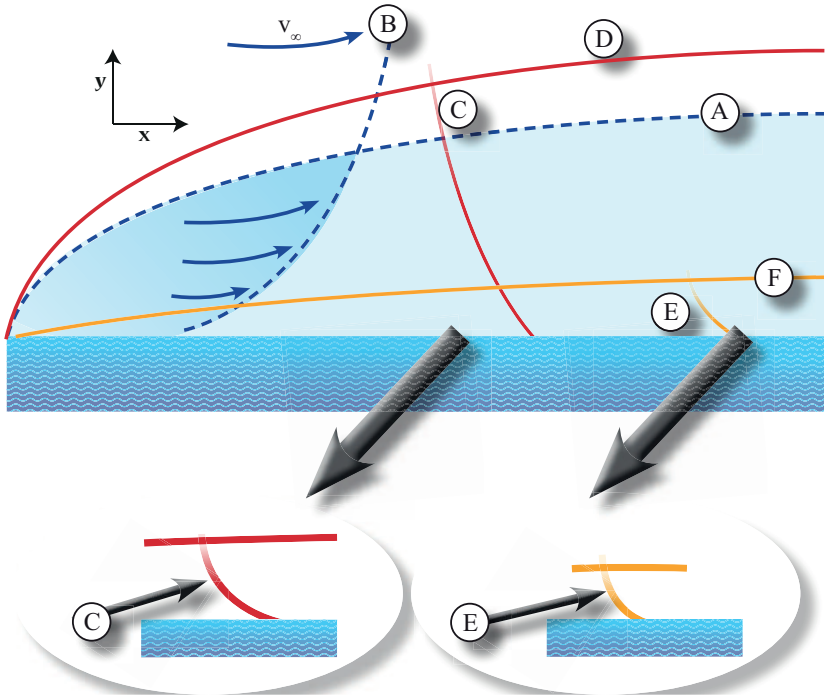

Figure 2.2: Three boundary layers formed on the pond surface

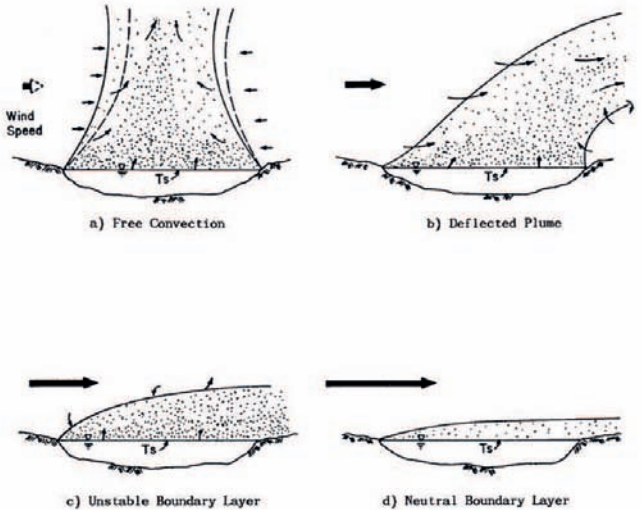

Figure 2.3: Evaporation regimes [4]

in Figure 2.3a) and driven by the effect of buoyancy from air heated above the heated water surface. The result is a plume of vapour above the water surface. The introduction of low speed winds at the pond surface will deflect this plume forming the pattern shown in Figure 2.3b. As the wind intensity further increases an unstable boundary layer develops. In this regime the vapour plume forms a definite boundary layer above the water surface. The wind is not completely dominant in all instances and as shown in Figure 2.3c this type of flow is typically characterised by random tufts of vapour being released along the boundary plume. Lastly, high wind speeds form a neutral boundary layer which has the distinct shape of a fully developed boundary layer (depicted in Figure 2.3d) and is completely influenced by the flow of air parallel to the water surface.

The classic approach to quantifying the heat transfer due to evaporation from pond surfaces involves the calibration of coefficients to generic equations via experimental studies. Conversely, modern tools such as CFD has the potential to predict in detail the conditions at the water surface. Validating such numerical models however, requires detailed experimental studies as shown by González-Real et. al. [24]. The task would be further complicated considerably by the presence of an unsteady uneven liquid surface which is subject to complex unsteady wind conditions. This renders the use of lumped correlations to describe evaporative heat transfer far more attractive for this work.

Lumped correlations which predict evaporation from free surfaces have been presented by numerous researchers. The basic equation is invariant, while variations are present in specific aspects for different applications. Branfield [5] describes evaporation from the 1802 paper by Dalton [25] as proportional to the difference in vapour pressure at the water surface and that in the surrounding air. Further, the observation is made that the addition of wind to a water surface will affect the evaporation rate proportionately. This description leads to the general form of correlations representing the average heat transfer due to evaporation ($\overline{q}_{evap}$).

$$\overline{q}_{evap} = (a + bv_{\infty}^{n})\,(\Delta c_{vapour}) \tag{2.2}$$

where a is the constant of proportionality for free convection, b the proportional increase in heat transfer due to wind and v_{∞} the free stream wind

speed. With certain correlations the influence due to wind is varied using a power relation n and the final parameter defining evaporation is the difference in vapour concentration between the pond surface and free stream (Δc_{vapour}).

Using the above equation as basis, Adams et.al. [4] and Yilmaz and Aybar [26] employ a correlation first proposed by Geyer et.al. [27].

$$q_{evap} = \left(70 + v^2\right)(e_s - e_\infty) \tag{2.3}$$

where, e is the vapour pressure with the subscript s and ∞ denoting the pond surface and free stream. The coefficients were calibrated in Texas and Louisiana, no details of the measurements were however provided. Yilmaz and Aybar [26] suggests that the Brady equation can be used as a low estimate of evaporation from a pond surface. When however considering Equation (2.3) the coefficients do not change with varying atmospheric conditions and the correlation therefore does not account for the changing properties of the air above the water surface. This was corrected by Ryan and Harleman [28] from which the so-called Ryan Equation resulted:

$$q_{evap} = (2.7\Delta\theta_v^{\frac{1}{3}} + 3.1v)\frac{e_s - e_\infty}{100} \tag{2.4}$$

Unlike the Brady Equation, the Ryan Equation accounts for the virtual temperature difference ($\Delta\theta_v$) in the free convection term. The virtual temperature of a moist parcel of air is the temperature at which a theoretical dry air parcel would have a total density and pressure equal to the moist parcel of air [29]. It is calculated as:

$$\theta_v = \frac{T}{1 - \frac{0.378e}{P_a}} \tag{2.5}$$

where T is the temperature of the air. In Equation 2.5 vapour pressure is denoted as e and atmospheric pressure as P_a. The vapour pressure is calculated using the fluid property correlations presented in Appendix B, Equation (B.5). Finally, the effect of relative humidity (Φ_{rh}) is accounted by:

$$e = \Phi_{rh} P_{vapour} \tag{2.6}$$

The Ryan Equation is suggested by Yilmaz and Aybar [26] as the upper estimate for evaporation when using the Brady Equation as the lower estimate. The experimental coefficients derived for the Ryan Equation were established from tests conducted at the Hazelwood Cooling Pondage in Australia. The region was visited by the author, and it was found that similar atmospheric conditions to that at Matimba Power Station are prevalent. The pond has a surface area of $5,000,000\ m^2$, making it approximately 20 times larger than the ponds at Matimba Power Station. The Ryan Equation was also tested in the study by Adams et.al. [3] on the pond at East Mesa (located in the USA in a region where climatic conditions are similar to the arid conditions in Lephalale, where temperatures often exceed $35°C$) with a surface area of $3,600\ m^2$ and found accurate to 15%.

Adams et. al. [3] were further able to improve the above correlation. As also noted by Brutsaert [30], Sherman and Webster [31] and Webster and Condie [32], the average evaporation rate decreases as the size of the water body increases. The term used to describe the variance due to size is called the fetch. Harbeck [33] proposes a correlation for forced convection whilst taking the fetch into account by including the pond surface area (A). The correlation was developed from experimental studies on water bodies with surface areas ranging from $4 \times 10^3\ m^2$ to $121.4 \times 10^6\ m^2$. The studies were conducted in various climatic conditions. Bearing this in mind, Adams et.al. [3] use this fetch dependent forced convection term to modify the Ryan Equation. The vector sum of the free convection term from the Ryan Equation and the forced convection term by Harbeck [33] then make up the heat flux in the New-Ryan Equation:

$$q_{evap} = \sqrt{\left(2.7\Delta\theta_v^{\frac{1}{3}}\right)^2 + \left(5.1\left(\frac{A^{-0.05}}{10000}\right)v\right)^2}\,\frac{e_s - e_\infty}{100} \tag{2.7}$$

The most recent work which assessed the effect of fetch is by Cook et. al. [34]. This comparative analysis of correlations which correct the heat exchange rate based on the effects of fetch suggests that the following correlation rather be used:

$$q_{evap} = \frac{(2.36 + 1.67v)\, A^{0.95} \rho_{water} L_v}{8.64 \times 10^7} (e_s - e_\infty) \tag{2.8}$$

where L_v is the latent heat of vaporisation. In passing it is noted that Cook et. al. [34] cautions the reader on the applicability of the correlation by Harbeck [33]. According to McJannet, measurements taken at land-based stations are not applicable for use with the correlation by Harbeck [33], however the study did not consider the application of the Harbeck correlation in the New-Ryan Equation, which had been experimentally validated through the study by Adams et.al. [3]. Land-based measurements from these experiments provided reliable input parameters for an accurate prediction of evaporation from a free surface. The last fetch-dependent correlation considered is presented in a critical review of evaporation equations by Sartori [23]. The investigation evaluates various evaporation equations and suggests that Equation (2.9) is used for evaporation from a free surface.

$$\dot{m} = \left(0.00407 v^{0.8} L^{-0.2} - 0.01107 L^{-1}\right) \frac{(e_s - e_\infty)}{P_a} \tag{2.9}$$

where L is the length of the pond in the direction of the wind and P_a is the atmospheric pressure. The correlation is fetch dependent, however unlike the correlations presented by McJannet [34] and Harbeck [33], fetch is accounted for by the length of of the flow path. Sartori [23] does not provide details of the test conditions for these equations and therefore its applicability to this study is unclear, and the correlation is not considered further.

The next significant study on describing evaporation is that by Branfield [5] whom employs theory developed by Kröger [35] to develop an alternative correlation. The correlation is derived from the diffusion of a substance at a surface together with the assumption of a semi-infinite solid. The result is a correlation that includes all atmospheric parameters which effect evaporation, which will be referred to as the Kröger Equation.

$$q_{evap} = \left(\frac{C_f \frac{g\mu^2(\rho_{avs} - \rho_{av\infty}) c_{p(av)}}{k\rho_{vave}^2}^{\frac{1}{3}}}{Sc} + \frac{0.0052 v_\infty}{2 Sc^{\frac{2}{3}}} \right) \frac{p_{vs} - p_{v\infty}}{R_v T_{film}} L_v \tag{2.10}$$

where μ, ρ and k are the dynamic viscosity, density and conductivity of the fluid respectively, g the gravitational acceleration and C_f the experimentally derived skin friction coefficient which was estimated to 0.2106. Further Sc denotes the Schmidt number, L_v the latent heat of vaporisation and R_v the universal gas constant for vapour. The experiments used to calibrate these coefficients were conducted on films of water with the dimension $1m \times 1m$. When analysing correlations for the ECP, the dimensions are important as this effects aspects such as fetch. The derivation of the Kröger Equation shows that the free convective term is non-dimensional via the use of the Rayleigh number:

$$Ra = \frac{g\beta(\Delta T)x^3}{\nu k} \tag{2.11}$$

where β is the thermal expansion coefficient, ΔT the temperature difference between the surface and air, ν the kinematic viscosity of the fluid and k the thermal conductivity of the fluid. These terms are simplified to use measurable parameters in Equation (2.10). In the derivation by Kröger [35] the proportionality between the Rayleigh and Nusselt (Nu) number is set as:

$$Nu \propto Ra^{1/3} \tag{2.12}$$

The selection of this proportionality eliminates the length dimension (x) from the equation and therefore can be considered independent. Considering now the Ryan Equation, the virtual temperature difference ($\Delta\theta_v$) is raised to the exponent 1/3 which is also related to the Rayleigh Number. Therefore the Ryan, New-Ryan and Kröger Equations all include a non-dimensional free convective component for evaporation which will be considered when comparing the applicability of the correlations.

To complement Equation (2.10), the following relation is employed in the case when the water surface temperature is lower than ambient, Branfield [5] suggests:

$$q_{evap} = \left(\frac{0.0093}{\rho_{av} c_p} + 6.7 \times 10^{-6} v_w\right) \frac{(p_{vs} - p_{v\infty})}{T_{ave}} \tag{2.13}$$

Having listed and discussed the available lumped evaporation models, the next task is to select the most appropriate for the ECP under investigation. This is detailed in the section to follow.

2.1.2 Evaluation and Validation

The ponds located at Matimba Power Station are large and access to experimental data of such a pond is challenging. The quantity of energy needed to heat up a body of water as large as the ponds at Matimba Power Station is impractical. Furthermore, the wind speed at various heights and locations; pond water and air temperature at various positions and measurements of the relative humidity are needed for a thorough experimental study. Consequently, ponds detailed in the literature were to be modelled in order to assess a selection of candidate correlations (from those listed above). The first of these pond studies is due to Athey et.al. [7]. The latter provides relatively detailed experimental data for a large pond located at East Mesa in California, USA. The tests were conducted for the experimental study by Adams et.al. [3], where the results from the experimental study were used to estimate evaporation from a free surface (This data is given in Appendix C).

The East Mesa pond has a surface area of $3600m^2$ and a depth of $1.5m$. Therefore the pond surface area is greater than the depth by more than three orders of magnitude. This is characteristically similar to the pond at Matimba Power Station that implies heat exchange is dominant at the pond surface. Another similarity lies in that the East Mesa pond is lined. During the experiment, water was heated to temperatures approaching $50°C$ and left to cool. The elevated surface temperature implies that the pond cools due to mainly evaporative heat transfer.

During the East Mesa tests, water temperature was measured at nine separate locations on the pond and the average value published. Air temperature and wind speeds were measured on two towers in the region. Measurements of the relative change in water level was also measured throughout the experiment. Details of the measurements taken are shown in Table 2.1.

Evaporation cannot be directly measured from a large pond. Two methods for estimating this were therefore used in the study by Adams et.al [3], namely the Water Balance and Energy Budget methods for evaporation estimation. The Water Balance method uses Equation (2.14) for this purpose as:

Table 2.1: Data Provided by Hadlock [7]

Description	**Units**
Pond Temperature	$^{\circ}C$
Surface Elevation	cm
Short wave Radiation	W/m^2
Net Radiation	W/m^2
Tower 1 Wind Speed ($1.5m$ agl)	m/s
Tower 2 Wind Speed ($4.8m$ agl)	m/s
Tower 1 Dry-Bulb and Wet-Bulb Temperature ($1.2m$ agl)	$^{\circ}C$
Tower 2 Dry-Bulb and Wet-Bulb Temperature ($1m$ and $2m$ agl)	$^{\circ}C$
Tower 2 Dry-Bulb and Wet-Bulb Temperature ($4.8m$ and $9m$ agl)	$^{\circ}C$

$$\Delta V_{evap} = -\Delta V_{pond} + \Delta V_{flow} + \Delta V_{precip} \tag{2.14}$$

where ΔV is the change in volume, the subscripts $evap$, $flow$ and $precip$ represent the mass transfer via evaporation from the pond, flow to and from the pond and precipitation added to the pond. During the test, the pond level is measured using a hook gauge from an arbitrary datum. This is used to calculate the change in pond volume ΔV_{pond}. Since water flow through the pond is ceased before the experiment starts and tests are conducted during periods with no precipitation, ΔV_{pond} is the only measurement affecting the change in pond volume and directly relates to water loss as a result of evaporation.

The measurement of the change in volume ΔV_{pond} introduces an inaccuracy significant to the results of this study. During the experiment the pond will experience a change in density as a result of the liquid cooling. This density change is small (approximately 0.78%), however when compared to the magnitude of water lost through evaporation, this quantity remains significant. Therefore, the water volume is corrected through the use of temperature measurements of the piping leading to the hook gauge instrument measuring the pond level. This variance is shown in Table 2.2 and the correction is appropriately included by Adams et.al. [3].

Table 2.2: Apparent vs Actual Evaporation [7]

	Apparent Volume (m^3)	Actual Volume (m^3)	Water Loss Apparent (m^3)	Water Loss Actual (m^3)	Error ΔV (m^3)	Δh (m^3)
Initial	4727.6	4727.6	–	–	–	–
1 hr	4718.3	4719.8	9.3	7.8	1.8	0.08
24 hr	4581.5	4608.7	140.0	118.9	21.1	0.82

Considering the Energy Budget methodology next, the water body is considered as a control volume. All in and out flows of energy, excluding the evaporation and thermal convection are estimated over a finite period.

$$Q_{evap} = \frac{-\Delta Q_{stored} + Q_{sol} + Q_{rad} + Q_{conv} - Q_{flow}}{1 + \overline{R}} \tag{2.15}$$

where ΔQ_{stored} is the change in stored energy, Q_{solar} is the net incoming solar radiation, Q_{rad} is the net radiation, Q_{conv} the heat exchange by thermal convection, Q_{flow} the energy from in and outflows and $\overline{R}$ is the Bowen ratio which relates the convective and conductive properties of the fluid. The thermal convection is indirectly calculated. The indirect estimation of convection is done through an energy budget analysis using the evaporation calculated from the Water Balance method. Considering the many approximations in addition to the Energy Budget being reliant on the Water Budget, the former was disregarded and the Water Budget employed for the purpose of evaluating correlations.

The second experiment considered for validation was that detailed by Branfield [5]. The tests were conducted on a film of water with a surface area of $1m^2$ placed in the natural environment. Measurements of the water temperature, ambient air wet and dry bulb temperatures, wind speed and solar radiation were recorded. Measurements of the water loss was periodically recorded and the lost water is replenished after each measurement. This water added was at the same temperature as the film of water to ensure that it does not affect the evaporation rate. For further information on the details of this experiment, the reader is referred to the thesis by Branfield [5].

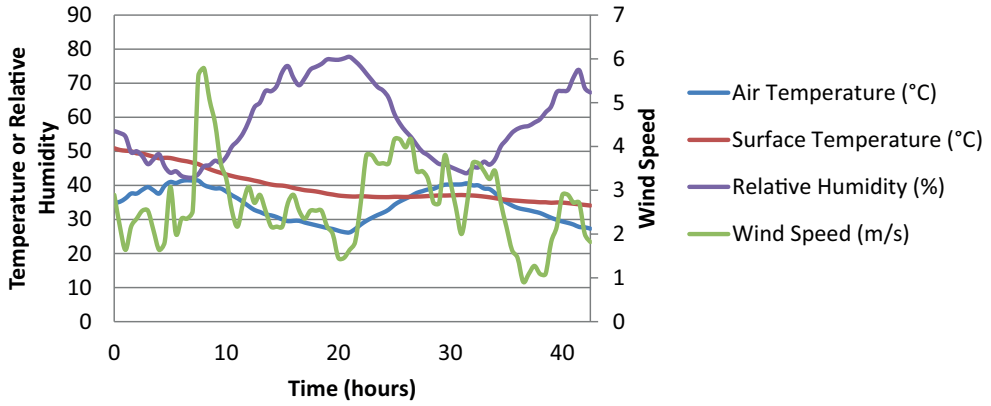

Figure 2.4: Experiment 4 Atmospheric Data

The experimental data for the two experiments described above provide the necessary input for the comparative assessment of the correlations found in literature. The vast difference in size between the East Mesa pond and the experimental apparatus used by Branfield can be used to show the applicability of these equations to various sized water bodies. This is of particular interest in this work, as the main unique aspect of the pond under consideration is its size.

Using the data from the East Mesa experiment, the pond temperature for each discrete time step is prescribed and the evaporation rate is predicted. This rate is then compared to the evaporation rate measured in the Water Balance from the study by Adams et.al. [3]. The ambient conditions during Experiment 4 [7] is shown in Figure 2.4. The correlations identified in the Literature Study were developed for wind speeds measured $2m\ agl$, therefore a logarithmic profile assumption as done by Adams et. al. [3] is used to correct the wind speed. While numerous formulas are available for this purpose, Adams suggests that Equation (2.16) provides reasonable accuracy for engineering studies.

$$\frac{v_1}{v_2} = \frac{ln\frac{z_1}{z_0}}{ln\frac{z_2}{z_0}} \tag{2.16}$$

where v is the wind speed and z the height at which measurements are taken. The subscripts 1 and 2 represent the measurements taken and z_0

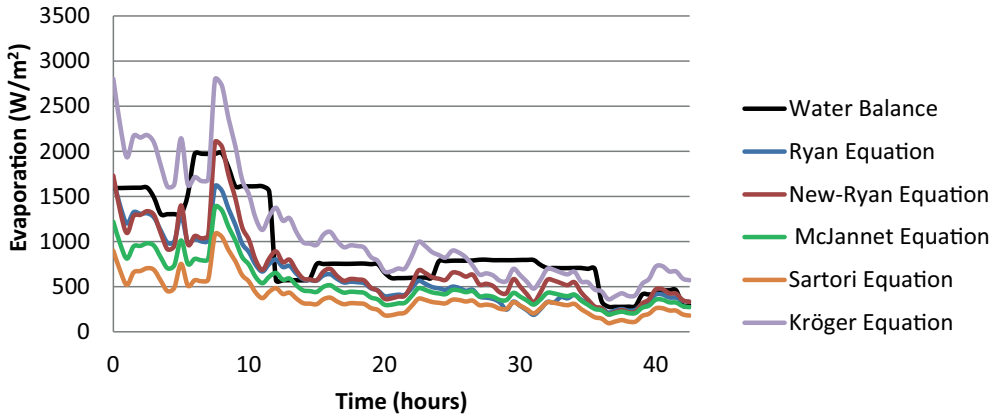

Figure 2.5: Predicted evaporation from the correlations in literature

is a representative indicator of the landscape surrounding the pond called the roughness height. For this application, if wind speeds are higher than $2.25m/s$, z_0 is $0.001m$, in instances where the wind speeds are greater then $2.25m/s$ the roughness height of $0.005m$ is applicable [3]. The wet-bulb temperature is measured during the experiment, this is used to determine the relative humidity using the formulation provided by Buck [36].

The input data were applied to the Ryan, New-Ryan, McJannet, Sartori and Kröger Equations to predict evaporation rates. These predictions are compared to the measurements from the Water Balance method in Figure 2.5. The figure shows that the Ryan and New-Ryan equations seem to predict evaporation most accurately. On the other hand, the Kröger Equation over-predicts evaporation significantly. This is likely a result of the coefficients being developed in an experiment on a significantly smaller body of water. The result clearly shows that the Sartori and McJannet Equations under-predict evaporation by a significant margin.

Next the cumulative average error is calculated for each equation and shown in Figure 2.6. From this Figure it is clear that the New-Ryan Equation provides the most accurate prediction of evaporation. By in addition noting that it offers a conservative estimate, it was selected as the correlation of choice for this study.

Before the evaporative correlation selection can however be concluded, the reader is reminded that the ECP at Matimba Power Station is orders of

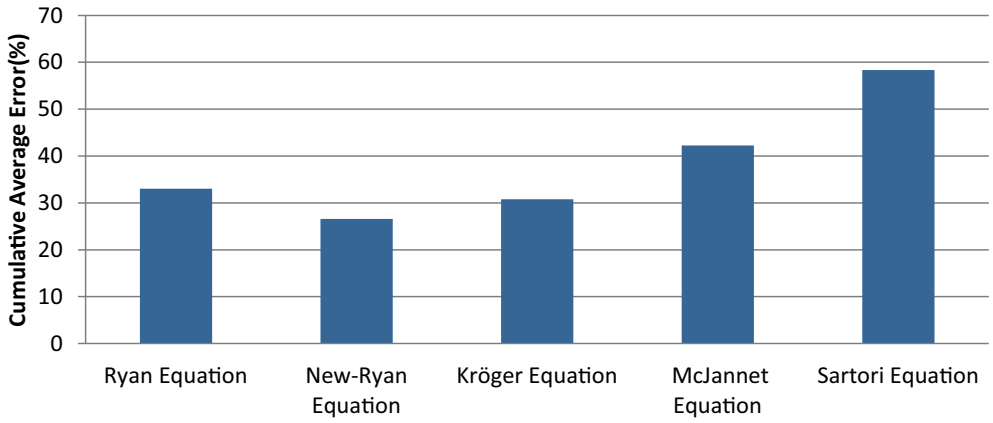

Figure 2.6: Average cumulative error for the predicted evaporation rate

magnitude larger than the pond at East Mesa. To this end, the New Ryan Equation is pitted against the others to assess ability to account for size variation. The Branfield [5] experiment is therefore modelled using the previously assessed correlations (with the omission of the Sartori Equation due to its weak performance). The input conditions from the experimental data used in the Branfield experiment is shown in Figure 2.7 below. These parameters are then applied to the Ryan, New-Ryan, Kröger and McJannet Equations to simulate the evaporation rate.

The results of the simulations are shown in Figure 2.8. The expectation that the Kröger Equation is most accurate for this apparatus is confirmed since the coefficients were calibrated using this experiment. The Ryan Equation now grossly under-predicts the evaporation rate from the water surface. The New-Ryan and McJannet Equations under predict evaporation by a smaller margin while being circa 80% accurate. This is remarkably accurate bearing in mind that the pond under consideration is three orders of magnitude smaller than the East Mesa pond. The superior accuracy of the New Ryan Equation for use in modelling the Matimba ECP is therefore confirmed.

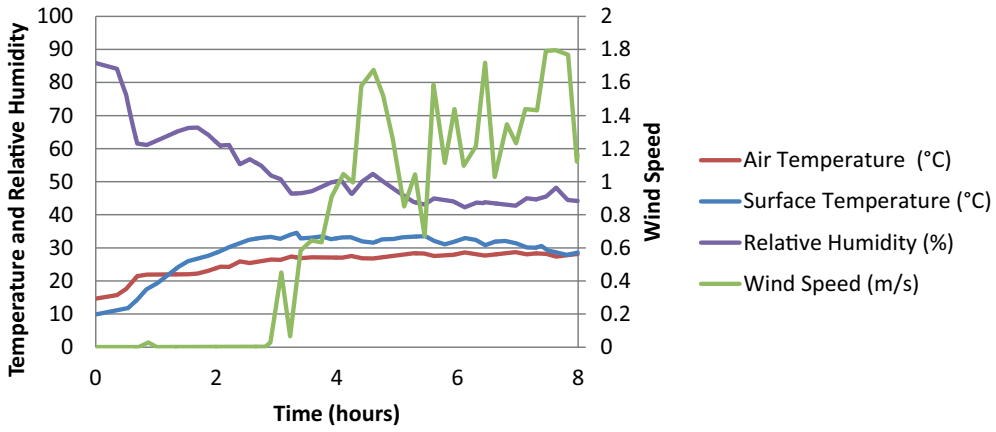

Figure 2.7: Input data for the Branfield Experiment [5]

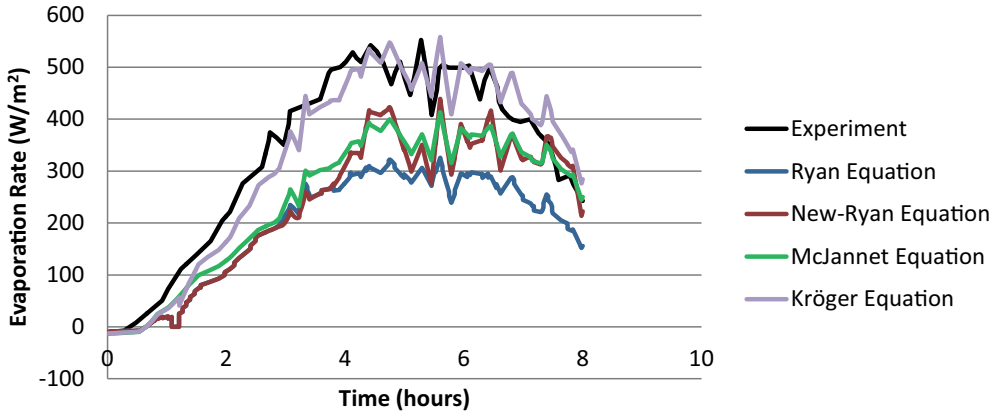

Figure 2.8: Predicted evaporation in the Branfield Experiment for correlations found in literature

2.2 Convection

The next medium of heat exchange considered is through thermal convection. As described in Section 2.1 flow over a flat surface will result in the development of a thermal boundary layer. The rate of heat transfer through this boundary layer is effected by the thermal conductivity of the air. The resulting heat transfer rate follows again by applying Fourier's law analogous to Fick's law. That is,

$$q_s'' = -k\frac{\partial T}{\partial y} \tag{2.17}$$

where k_f is the thermal conductivity of the air and $\frac{\partial T}{\partial y}$ is the temperature gradient at the surface. The development and characteristics of this boundary layer is similar to the evaporation boundary layer described previously. As a result of this similarity, the general formulation for convection is in the same form as that shown in Equation (2.2). The difference is naturally that heat transfer is driven by temperature and is known as Newton's law of cooling [22].

$$q_s = (const + dv)(\Delta T) \tag{2.18}$$

where *const* and d are experimentally derived constants representing free and forced convection respectively. Numerous studies available in literature have provided constants for the coefficients. Burger [37] notes that applying constants to the coefficients of this equation results in the correlation being restricted to specific applications. The cited work therefore concludes that the correlation presented by Kröger [35] should be tested. To this end an experimental test was conducted to determine the coefficients applicable to convection from a flat surface in the natural environment. The result is the following correlation:

$$q_{conv} = \left(0.2106\left(\frac{\mu T}{g(T_s - T_\infty)c_p k^2 \rho^2}\right)^{\frac{1}{3}} + v_w\left(\frac{0.0026}{2}\right)\left(\frac{c_p k^2 \rho^3}{\mu^2}\right)^{\frac{1}{3}}\right)\Delta T \tag{2.19}$$

where c_p is the specific heat, k the thermal conductivity, μ the dynamic viscosity and ρ the density of the air above the water surface. This equation was the basis for the Kröger Equation used in Section 2.1 above. The study by Burger [37] also investigated convection coefficients during night time and produced the following relationship:

$$q_{conv} = \left(3.87 + 0.0022\left(\frac{v\rho c_p}{Pr^{2/3}}\right)\right)\Delta T \tag{2.20}$$

where Pr is the Prandtl Number. These two correlations were developed through a rigorous mathematical analysis of a semi-infinite surface and therefore independent of dimensions. Sartori [38] also critically assess correlations for convection from flat surfaces. In this analysis various correlations published in literature were tested and the conclusion of the analysis showed that the correlation presented below was the most reliable prediction for thermal convection.

$$\begin{aligned} q_{conv} &= (3.83v^{0.5}L^{-0.5})\Delta T \text{ (laminar flow)} && (2.21)\\ &= (5.74v^{0.8}L^{-0.2})\Delta T \text{ (fully turbulent flow)} && (2.22)\\ &= (5.74v^{0.8}L^{-0.22} - 16.46L^{-1})\Delta T \text{ (mixed flows)} && (2.23) \end{aligned}$$

However, the study was aimed at applications where predictions for convection from smaller surfaces, such as solar panels, was required. All the equations described by Sartori [38] use correlations which incorporate constants for the coefficients of convection. A list of the equations assessed by Sartori are as follows:

$$\begin{aligned} q_{conv} &= (5.7 + 3.8v)\Delta T && (2.24)\\ &= (2.8 + 3v)\Delta T && (2.25)\\ &= (4.5 + 2.9v)\Delta T && (2.26)\\ &= (9.4v^{\frac{1}{2}})\Delta T && (2.27) \end{aligned}$$

Assessing the most appropriate correlation for this application required the selection of a correlation applicable to the specific conditions found at Matimba, while the above correlations were generally developed in controlled

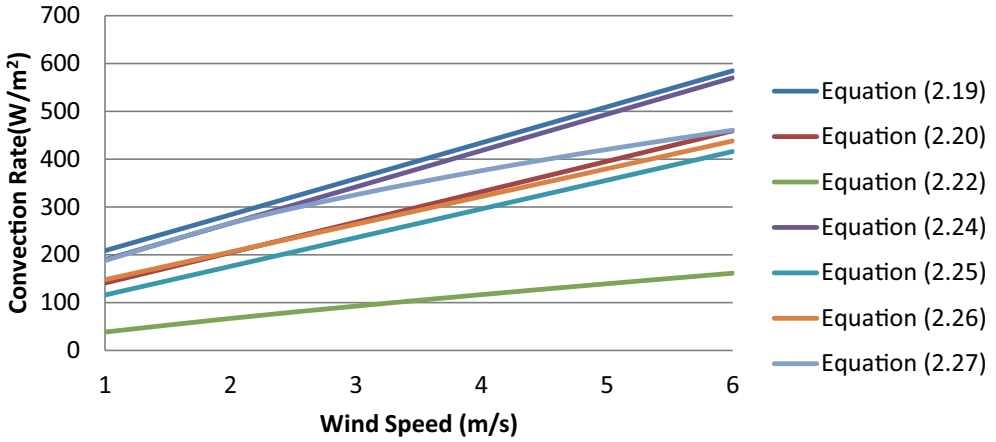

Figure 2.9: Comparison between convection coefficients

conditions on very small plates. Therefore the equations that seems most promising (due to their non-dimensional nature) are (2.19) and (2.20).

The heat exchange rates are compared, with respect to varying wind velocities are compared in Figure 2.9 for the general instance where there is a $20K$ difference in temperature between the pond surface and air. Equation (2.10) is found to predict the highest convection rate, while Equation (2.21) predicts the smallest convection rate. Equations (2.24) to (2.27) are found to lie between these boundaries. Equations (2.10) and (2.13) were developed for prediction of convection in large scale systems (Pretorius [39]).

With the information available, the author opted to select Equations (2.10) and (2.13), noting that this is the least conservative of the equations presented. Equation (2.21) is disregarded as its application by Sartori [38] was based on shorter length scales and application to the large cooling pond is likely to grossly under predict convection. The remaining equations are similar in magnitude. Since the net effect of convection is orders of magnitude smaller than evaporation, it is expected that the effect on the pond temperature between correlations would be negligible. Therefore the effect of Equation (2.26) on the final pond temperature will be compared to that using Equations (2.10) and (2.13). It is expected that the variance is negligible.

2.3 Radiation

Radiation is the transfer of heat between two bodies with different temperature without the use of a heat transfer medium. Radiant energy from the sun (Solar Radiation) would heat the pond surface adding energy to the pond. The temperature difference between the pond surface and the sky (Atmospheric Radiation) will drive heat away from the pond. The two types of heat transfer by radiation can be individually investigated.

2.3.1 Atmospheric Radiation

Atmospheric radiation heat transfer is typically a function of the temperature difference between the water surface and the surround environment. The exchange is fundamentally quantified by the Stefan-Boltzmann constant (σ) and the sky temperature. The sky temperature is not a quantity that is measured and therefore the equation is simplified by using the ambient air temperature in conjunction with an empirical value for emissivity ϵ.

$$q_{sky} = \sigma T_{sky}^4 = \sigma \epsilon_{sky} T_a^4 \tag{2.28}$$

where T_{sky} is the effective clear sky temperature and T_a is the ambient air temperature near the ground. Researchers typically approximate the sky emissivity as a function of the ambient dew point temperature. Burger [37] assessed various correlations experimentally. The experimental procedure rigorously measured radiation from a flat surface which was maintained at a constant temperature. The heat exchange as a result of radiation could then be measured and the results compared to correlations found in open literature. The correlation deemed most accurate (and therefore selected for this study) is that by Fromberg and Berdahl [40]

$$\epsilon_{sky} = 0.741 + 0.0062 T_{dp} \text{ (day)} \tag{2.29}$$

$$= 0.727 + 0.0060 T_{dp} \text{ (night)} \tag{2.30}$$

These equations are valid for clear sky conditions. This was selected as

the absence of clouds would result in the highest solar radiation (which is considered in the next section).

2.3.2 Solar Radiation

Solar energy entails the addition of heat from the sun. Numerous researchers have looked at the effect of solar radiation on large surfaces. A noteworthy correlation is presented by Duffie and Beckman [41]. This correlation was successfully implemented by Chiasson [18] in an experimental assessment on heated ponds. The calculation requires the measurement of solar heat input which is measured using pyranometers. This information together with the position of the sun allow for the computation of the energy added by the sun to the surface. It is assumed that all heat from the sun is absorbed into the pond except the heat that is reflected.

The quantity of solar radiation reflected at the surface is computed by calculating the suns angle of incidence (θ) at each time step. The angle of refraction (θ_r) is calculated at each time step using Snell's law [41]. The reflectance (ρ') is calculated from:

$$\rho' = \tau_r - \tau \tag{2.31}$$

where τ_r and τ represent the refracted transmittance, reflected beam from the surface:

$$\tau_r = e^{\frac{\mu' d}{\cos\theta_r}} \tag{2.32}$$

$$\tau = \frac{1}{2}\left(\frac{1-r_{\parallel}}{1+r_{\parallel}} + \frac{1-r_{\perp}}{1+r_{\perp}}\right) e^{\frac{\mu' d}{\cos\theta_r}} \tag{2.33}$$

where d is the pond depth and μ' the extinction coefficient, un-polarised radiation in the parallel $r_{\parallel}$ and perpendicular $r_{\perp}$ direction are calculated from:

$$r_{\parallel} = \frac{tan^2(\theta_r - \theta)}{tan^2(\theta_r + \theta)} \tag{2.34}$$

$$r_{\perp} = \frac{sin^2(\theta_r - \theta)}{sin^2(\theta_r + \theta)} \tag{2.35}$$

The result allows for the calculation of solar heat transfer as function of time of day using the measured solar beam radiation (I_b) and diffuse radiation (I_d) as:

$$q_{solar} = (I_b \cos(\theta) + I_d)(1 - \rho')A_{pond} \tag{2.36}$$

The procedure utilising Equations (2.31) to (2.36) is used for this study based on the radiation information available. This is implemented as functions into the final pond model and added to the lumped thermal model as a negative heat term as it opposes the heat being rejected from the pond.

2.4 Ground Conduction

The thermal profile of soil below the pond surface will drive heat exchange by conduction. When compared to the other heat exchange modes, conduction is expected to be small in magnitude and its effect may not be significant to the performance of the ECP. Models which quantify the heat lost through a pond base via conduction is influenced by the composition of the pond floor and the flow of water through the pond floor. For the ponds at Matimba Power Station, the floor is lined with a rubberised canvas. This prevents water from seeping to the ground and the only means of heat exchange is as a result of conduction.

The rate of heat exchange via conduction can be estimated using the heat conduction equation (2.37). For a lined pond two methods were identified. Firstly, Chiasson [18] quantifies heat transfer by assuming that the rate of heat exchange is directly linked to the temperature difference between the water body and water in the water table. However, information relating to the depth of the water table and the temperature of the water is not freely

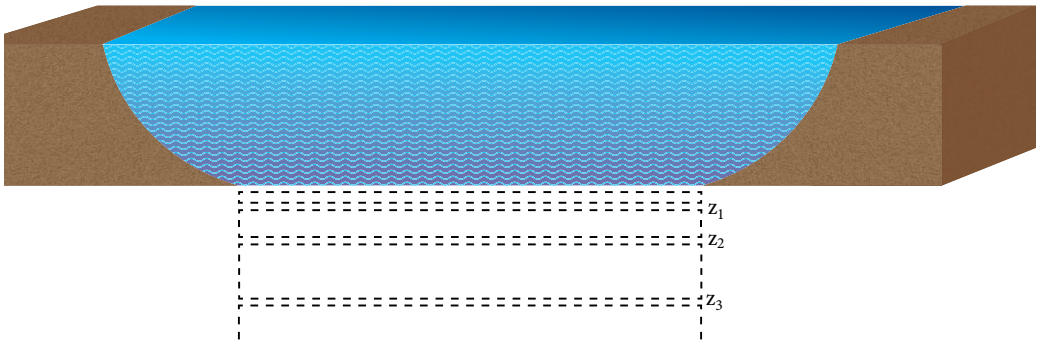

Figure 2.10: One dimensional finite difference mesh for the conduction of heat through soil

available. The second method involves the numerical solution of Equation (2.37). The method used by Hedderwick [42] and Pretorius [39] requires only the soil properties and water temperature.

$$\rho c_p \frac{\partial T}{\partial t} = k \frac{\partial^2 T}{\partial y^2} \tag{2.37}$$

where ρ, k and c_p are the soil density, conductivity and heat capacity respectively. T the temperature of the soil, t is time and y the distance from the pond base along the normal to the base. The discretised elements are graphically shown in Figure 2.10. Elements are sequentially extended by a constant multiplication factor of 2.15 (Hedderwick [42]), to yield an accurate solution.

The boundary conditions are based on two assumptions. Firstly, the temperature of the soil at the node at the pond base is equal to the pond temperature.

$$T_1 = T_{pond} \tag{2.38}$$

The next boundary condition assumes that the change in pond temperature with depth will tend to zero. This is a reasonable assumption since the temperature at a reasonable depth below the pond would eventually be uniform.

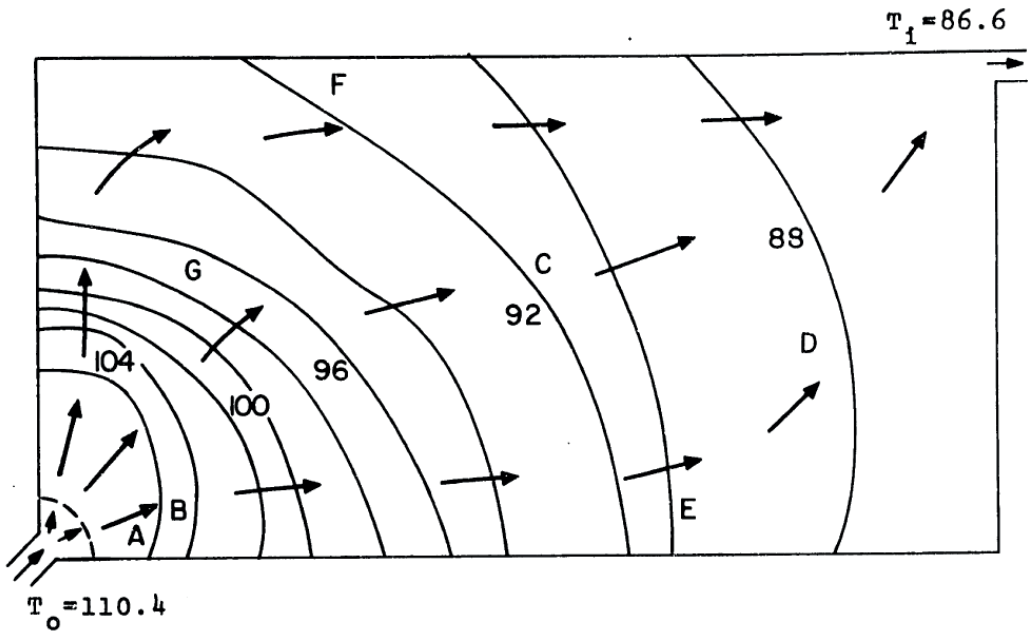

Figure 2.11: Typical Pond Profile [6]

$$\left.\frac{\partial T}{\partial y}\right|_{y=n} = 0 \tag{2.39}$$

The appropriate depth for accurate analysis was investigated by Hedderwick [42]. It was found that $16m$ would adequately estimate the soil temperatures for any time of the year. The above numerical procedure was therefore employed for the ECP pond model.

2.5 Heat Transfer in Water Body

The heat added from the condenser to the hot end of the pond will develop a thermal profile. Unlike traditional cooling ponds which are constantly operated, the pond at Matimba Power Station will have no active flow except during peak demand periods. During operation a thermal profile will develop. Cerco [6] shows typical pond temperature profiles based on experiments in Figure 2.11.

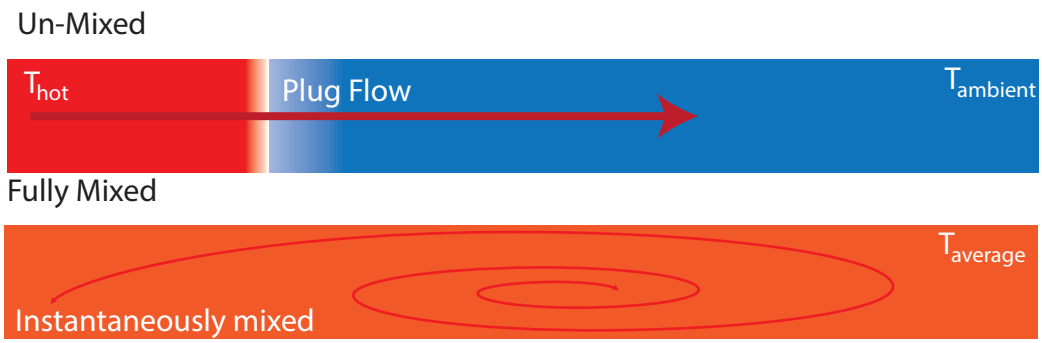

Figure 2.12: The pond mixing regimes

Similar to the latter, it is anticipated that Matimba Power Station pond will extract cold water from one end of the pond with heated discharge from the condenser entering at the opposite end. The result is a pond with a hot and cold region. However, once flow is ceased heat transfer in the horizontal plane is based on the influence of surface effects and the natural diffusion of heat in a still water body. CFD modelling of the resulting flow patterns can provide a detailed understanding of the thermal profile. However for this study a first approximation is employed as suggested by Jirka et.al. [14] and later proposed by Codell et. al. [21]. In their model, the cited authors propose three scenarios for flow in the pond, two of which are valid operating boundaries for this study.

Firstly, it is assumed that water entering the pond is instantaneously mixed and aptly named the "fully mixed" as shown in Figure 2.12. This will raise the average temperature of the pond water. Such a temperature rise will be small. The next scenario is described as plug flow which infers that hot water entering the pond will uniformly displace the cold fluid. The plug of hot water will not interact with the cold fluid and it will react independently with the environment. When analysing the unmixed regime for sequential operating cycles, the heat added from each subsequent cycle therefore will form independent regions as shown in Figure 2.13.

Through consultation with personnel developing the system for Matimba Power Station [8] the estimated operating parameters for the ECP system were provided as shown in Table 2.3. For the viability assessment of the ECP as a sustainable source of cooling, the requirement which was established by [8] is that the system should supply water to the condenser at a temperature lower than $30°C$ for ten consecutive days while being operated every second

Figure 2.13: Thermal profile of an unmixed pond after five operating cycles

Table 2.3: Operational information provided [8]

Thermal Load	$167 MW_{th}$
Mass Flow	$1600 \frac{kg}{s}$
Duration	3 hours
Surface Dimensions	$185\ m\ \times\ 235\ m$
Pond Depth	$3\ m$

day. This scenario was based on the data by Goldschagg [2] who reports that Vacuum Load Losses on consecutive days are experienced only 19% of the time. Based on the inputs provided in Table 2.3 the pond would operate for seven cycles for all the water in the pond to be circulated through the condenser.

Chapter 3

Numerical Model

The correlations described in Chapter 2 are now implemented into a computer model which will be used as a tool to predict the cooling rate for the pond at Matimba Power Station. This chapter describes the implementation of the model into a C++ programme. The programme has been designed to be modular and such that it may be used in future more detailed pond CFD studies. Units for input parameters have been standardised.

3.1 Numerical Model Formulation

The computer programme numerically solves Equation (1.2) using discrete Euler time steps, as shown in Equation (3.1). Initial conditions for each time step are used to calculate the fluid properties and heat flux for each mode of heat transfer during the time interval. Therefore it is assumed that the conditions are constant for the time step. This is accurate provided that small enough time-steps are used (which was the case in this study). The equations selected to calculate heat transfer for each time step are listed in Table (3.2). Once all parameters for the time interval have been calculated, T_{t_2} is determined by solving Equation (3.1).

$$\frac{T^{t_2} - T^{t_1}}{\Delta t} V \rho c_p = q_{evap}^{t_1} + q_{conv}^{t_1} + q_{rad}^{t_1} + q_{sol}^{t_1} + q_{ground}^{t_1} + q_{flow}^{t_1} \tag{3.1}$$

Table 3.1: Class input variables

Parameter	**Variable Name**	**Units**
Surface Temperature	`T_surface`	K
Ambient Air Temperature	`T_stream`	K
Wind Speed	`v_w`	m/s
Ambient Relative Humidity	`rh_stream`	%
Surface Area	`surface_area`	m^2
Day/Night indicator	`time`	$Boolean$
Atmospheric Pressure	`pressure`	Pa

where superscripts t_1 and t_2 represent the conditions and heat transfer rates at the beginning and end of each time interval, and Δt the length of the time interval. Each heat transfer mode, listed in Table (3.2), is programmed as a function and called to predict the pond temperature. The programme has a class called "`pond`" which takes conditions applicable to the pond (listed in Table 3.1) for a time step and calls the relevant functions which calculate the heat transfer from the pond. The fluid property data are taken from Kröger [1] and reproduced in Appendix B. Using this class allows the user to access the various correlations derived for this application presented in Section 2 (listed in Table 3.2).

The soil conduction is not included in the `pond` class. This is a heat transfer mode affecting the base of the pond and in cases where the internal convection patterns are being modelled, the vertical variation in temperature can be taken into account. Heat transfer from solar radiation is also separated from the `pond` class as the formulation used can vary depending on the type of solar information available. This programme currently uses measurements for the I_d, I_b and the incident angle of the suns rays on the pond surface (θ). Further, weather data for the years 2005 and 2006 were used for this study.

3.2 Programme Flow

The programme flow is shown schematically in Figure 3.1. All input files are space delimited text (`.txt`) files. Data for each input parameter are stored in vectors which the programme will access at each discrete time step. For

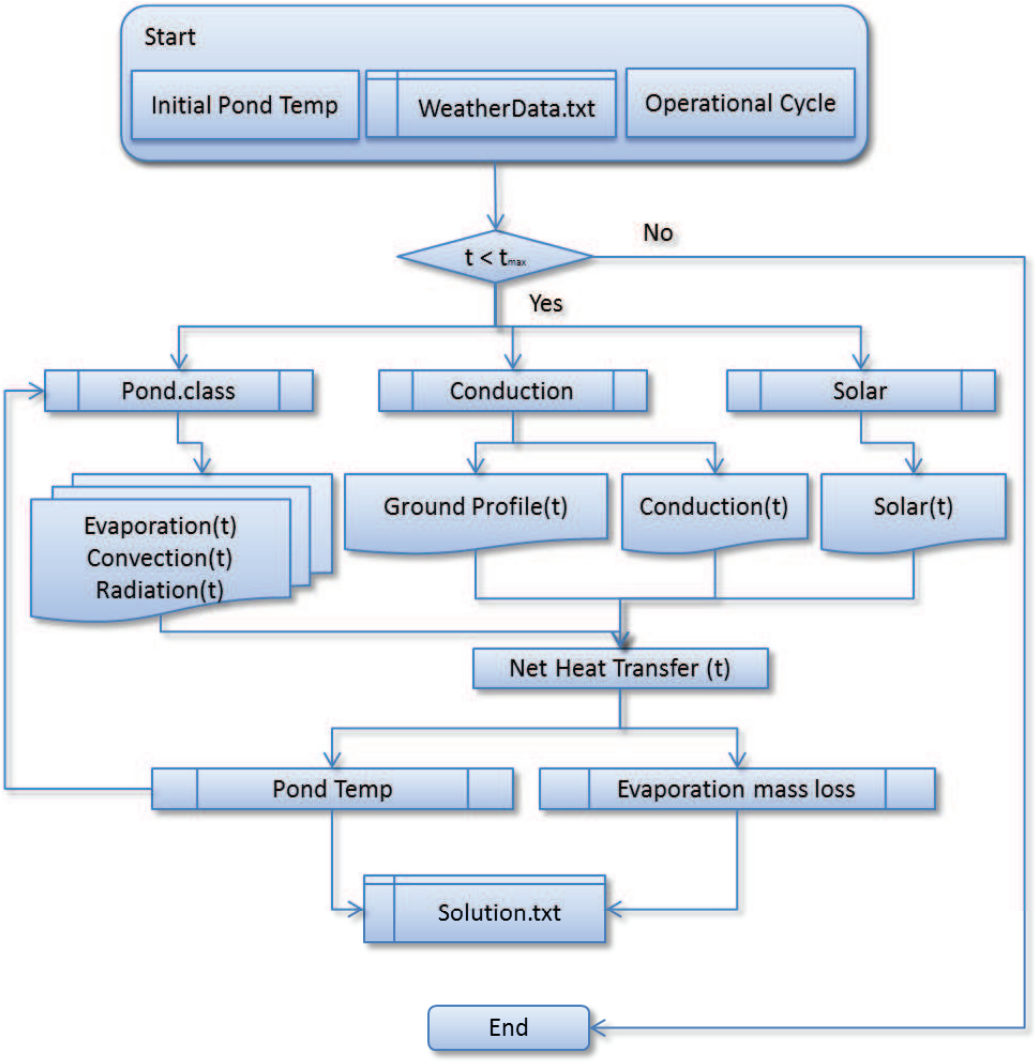

Figure 3.1: Basic programme flow chart

Table 3.2: Class output parameters

Type	**Name**	**Equation**
Evaporation	`Kroger()`	(2.10)
	`Ryan()`	(2.4)
	`Square()`	(2.7)
Radiation	`Radiation()`	(2.28)-(2.36)
Convection	`Conv()`	(2.19)
Sensitivity - Ryan	`rateQ_W_ryan()`	
	`rateQ_Ts_ryan()`	
	`rateQ_Ta_ryan()`	
	`rateQ_RH_ryan()`	
Sensitivity New-Ryan	`rateQ_W_New()`	
	`rateQ_Ts_New()`	
	`rateQ_Ta_New()`	
	`rateQ_RH_New()`	

this purpose the programme interpolates with-in the data set.The output files are also generated as comma delimited text files. The files output the primary information which is the pond temperature and water lost during each time step. For convenience the programme also outputs heat transfer rates of individual heat transfer modes and the input variables.

3.3 Programme Validation

The cooling rate of the East Mesa pond measured in the study by Athey et. al. [7] is now used to validate the developed programme. In short, this pond consists of a large water body with specific area similar to that at Matimba. It is heated to circa $50°C$ and allowed to cool naturally under similar weather conditions. All required input parameters were available in the publication and these may be implemented into the final computer programme to simulate a real ECP. In order to do this, the atmospheric data shown in Figure 2.4 was used.

The actual temperature change in the pond is compared to the predicted pond temperature in Figure 3.2 if the New Ryan equation is used for evapo-

Table 3.3: Class Output Parameters

Type	**Name**
Experiment 1	1.1%
Experiment 2	2.6% `Kroger()`
Experiment 3	0.77% `Kroger()`
Experiment 4	−4.7% `Kroger()`

ration. The result shows that the model predicts the ECP cooling rate with sufficient accuracy, the pond temperature is predicted to within $3.1°C$ (e.g. an average error of 5%). The prediction for Experiment 4 shown in Figure 3.2 is found to over-predict evaporation, and when the model was applied to the remaining three experiments it was found to be conservative. Table 3.3 shows the average error for the four experiments considered in this study. It is noted that in three of the four experiments the model provides a conservative solution.

The reason for this variance can be for numerous reasons. Given the information from the experiments, it was found that the average wind speed was particularly high in Experiment 4. This peak in wind speed is dominant during the beginning of the experiment. The sensitivity of evaporation is significant and therefore this would be expected. Hadlock [7] also showed that the direction of the plume relative to the weather station would affect the readings taken, unfortunately the wind direction was not recorded and therefore no further analysis could be conducted.

The contribution from each heat exchange mode is quantified in Figure 3.3, As expected evaporation is the largest contributor. It is particularly dominant during the initial period of cooling where the pond surface temperature is elevated.Radiation is the second largest contributor, and equals that of evaporation during mid-day

In Chapter 2 a rigorous analysis was conducted to select the equation most appropriate for evaporation. However there was a remaining degree of uncertainty in the prediction of the thermal convection. Therefore it was decided that using the least conservative equation would be compared to a reasonably conservative equation. Therefore the next simulation compares the pond performance when using Equation (2.26) and Equation (2.19). The result is shown in Figure 3.4.

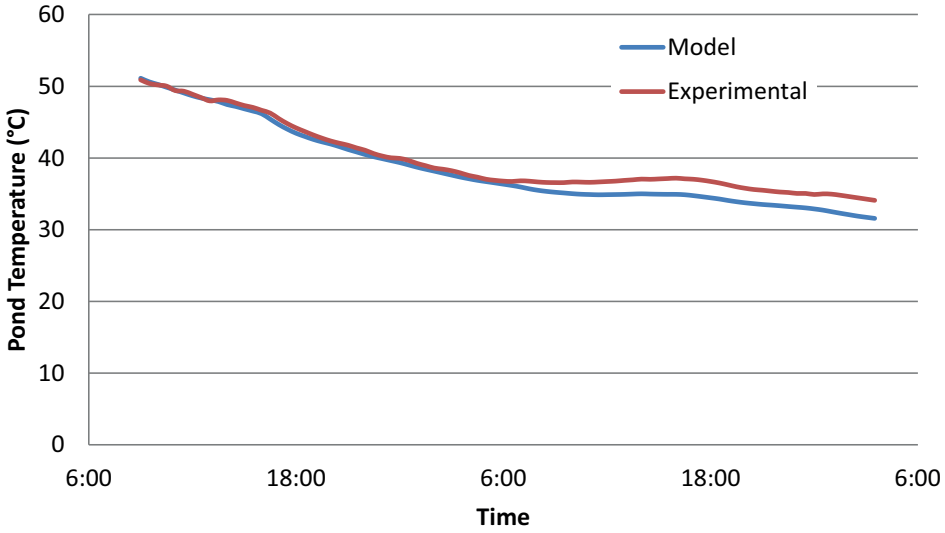

Figure 3.2: Predicted vs. measured pond temperature for Experiment 4

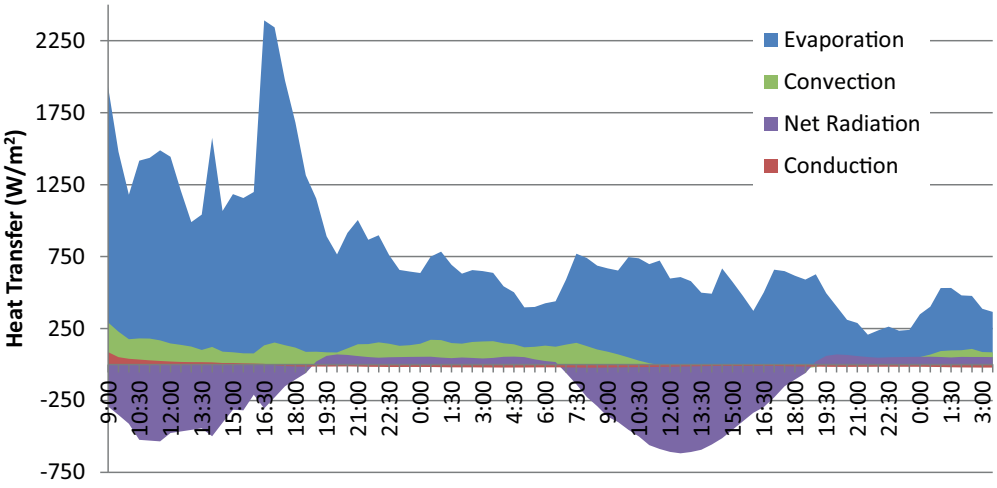

Figure 3.3: Contribution of the various modes of heat exchange

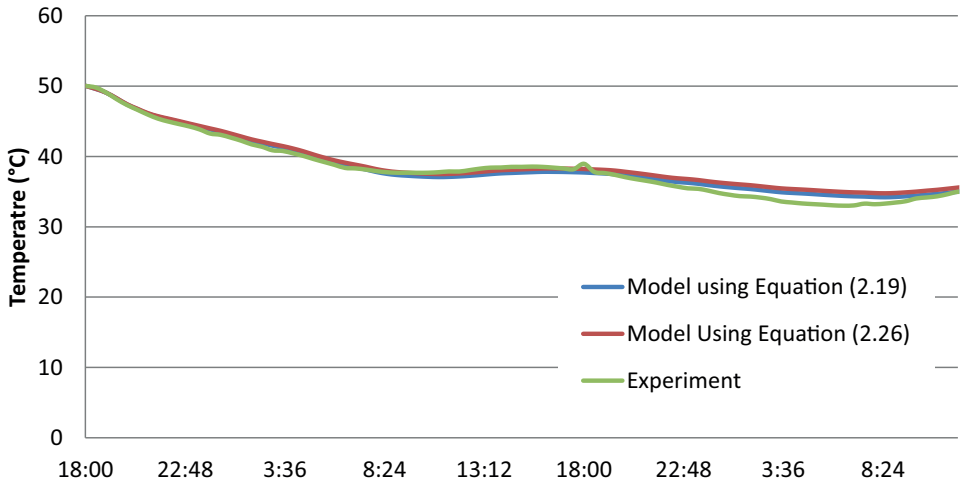

Figure 3.4: Pond cooling rate for Experiment 3 when using Equation (2.26)

The average difference between the pond temperature using the two different correlations is merely $0.3°C$, which is not deemed significant. Therefore the use of Equation (2.19) is acceptable for this application.

The final uncertainty deemed significant is that of the radiation input data. To assess the effect of this, input data was varied by 10% (up and down), and the resulting pond temperatures compared. This is shown in Figure 3.5 to be of little concern. The effect of radiation added to the pond when hot is graphically seen as a reduced rate of cooling.

In summary, the model developed for this study has proven to accurately predict ECP pond temperature evolution. The maximum difference between calculated and measure pond temperatures was $5°C$ or 4%. The developed model is therefore deemed suitable for application to investigating the viability of the Matimba ECP.

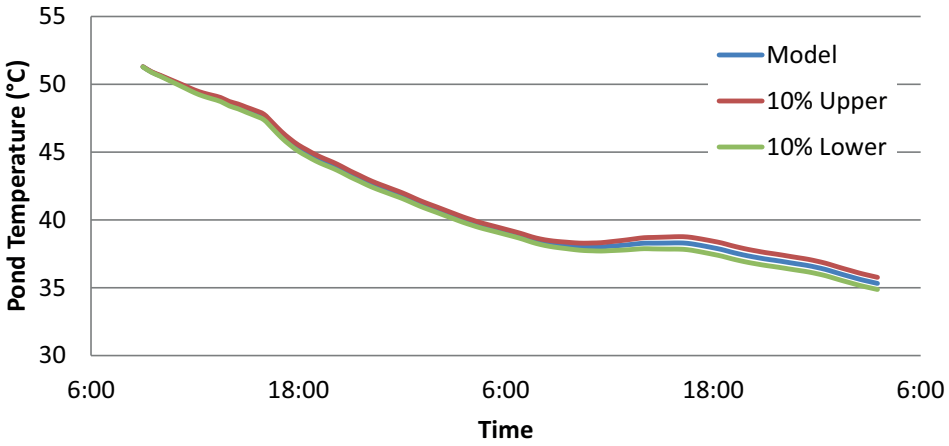

Figure 3.5: Effect of varying radiation for Experiment 3 on heat exchange

Chapter 4

ECP Viability Study

Using the numerical simulation tool, the thermal performance of a large cooling pond at Matimba Power Station is now simulated. Of particular interest is the time it would take for the pond to return to a sufficiently low temperature after being heated through operation, as well as the water lost due to evaporation. The results of this simulation will provide motivation for the further development of this particular system for implementation at Matimba Power Station.

The simulations used as input data captured via the plant's weather mast. The mast is located one kilometre west of the station and records air temperature and wind speeds at heights up to $40m$ above ground level. The weather conditions for a typical summer day with no precipitation is given in Figure 4.1. Since no measurements for solar input radiation were available for the Lephalale region, measurements taken in Upington [43] are used for this study. This is an over-estimation in the solar heat addition as it is on average 20% higher than that at Lephalale [44].

4.1 Pond Thermal Simulation

Detailed estimates by the utility suggest that the ECP system is intended to reject 167 MW of thermal energy to the pond. This is further to be done by pumping 1600 kg/s of water through the condenser when in use [8]. These

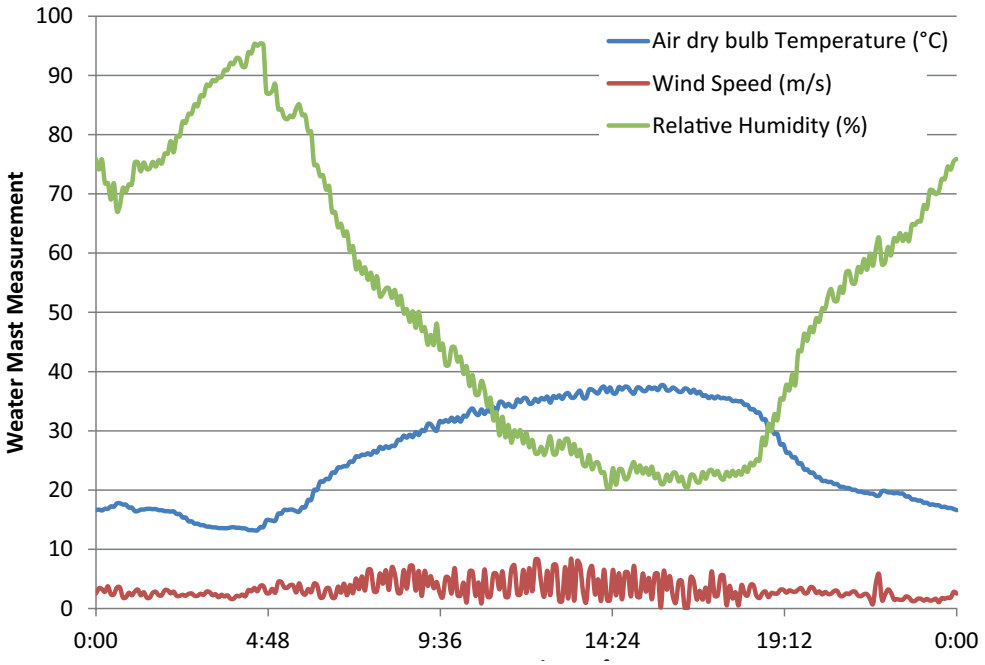

Figure 4.1: Ambient weather condition for a typical summer day

conditions will result in an estimated ECP temperature rise of 20°C within the condenser. The system is intended to only operate for discrete periods which last between two and three hours. Further, the target temperature to which to ECP is to be cooled is taken as 30°C.

In order to establish the least favourable month affecting the ponds performance, typical days of every second month were modelled. The time taken for a fully mixed pond and the heated plug of water in an unmixed pond after a single heating cycle the pond to return to the mean ambient temperature is compared in in Figure's 4.2 and 4.3. The result shows that the December atmospheric conditions are least favourable and as a result will be used for the simulations to follow. Importantly, the pond will return to the target temperature with-in 5 days of being heated (Figure 4.3).

Given the nature of the power system in South Africa, the peak demand for electricity is generally experienced between 17:00 and 20:00. A scenario where the ECP is used every alternate day for a ten day period was then investigated. By implication the $167MW_{th}$ is added to the ECP for three hours every second day. It was assumed for this study that water lost through evaporation is constantly replenished with water at the ambient temperature.

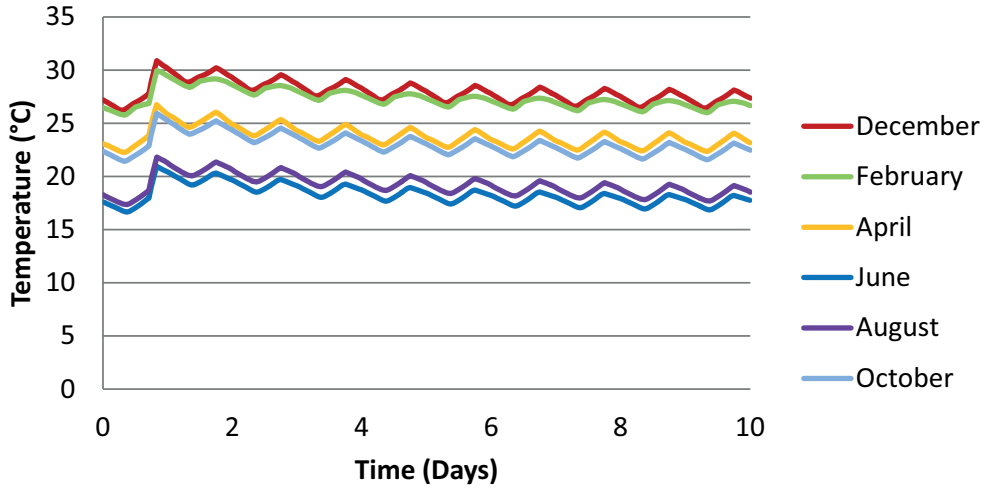

Figure 4.2: Pond cooling rate for various months of the year for a mixed flow model

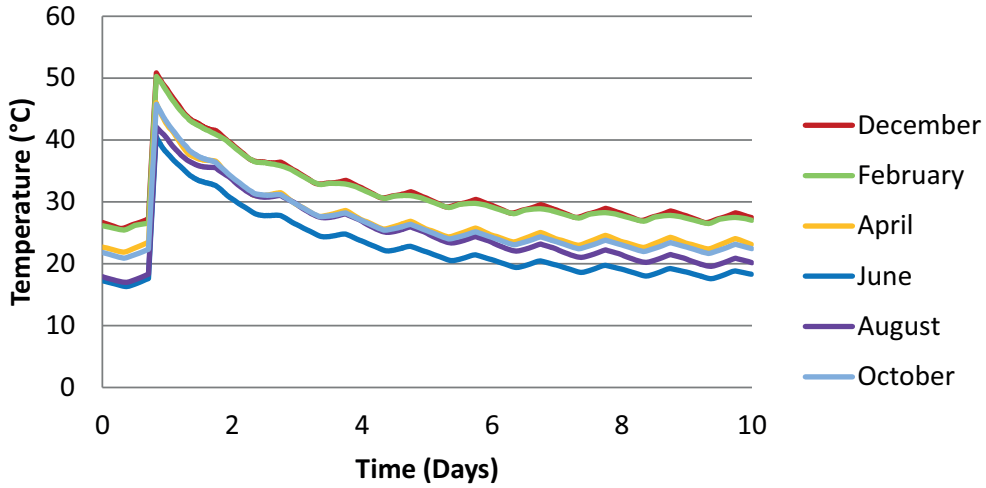

Figure 4.3: ECP cooling rate for various months of the year for an unmixed flow model

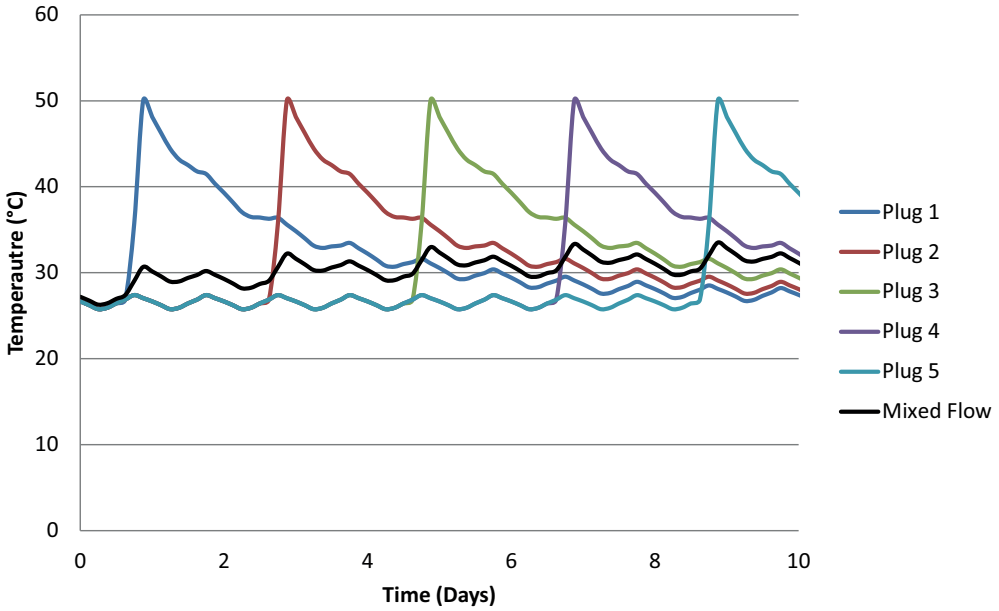

Figure 4.4: Typical performance of the ECP for 10 days

The resulting variation in pond temperature for a day in December is shown in Figure 4.4. Considering the plug-flow model first, water heated on the first day would have returned to a temperature of $27°C$ by the time it would be re-used. When using the mixed flow regime, the water temperature would have risen to $31°C$. Therefore the temperature of water at the discharge region of the pond will be between $27°C$ and $31°C$.

The reader is reminded that the wind speed was corrected using Equation (2.16) as wind measurements taken at Matimba are $10m$ agl. Figure 4.5 depicts the variation in pond temperature if the wind speeds were not corrected, and it is clear that the effect of the actual wind experienced at the ground being similar to that at the weather mast measurement point would favour the cooling rate.

The solar data used are based on measurements from Upington. As Lephalale experiences approximately 20% less incoming solar radiation on an annual basis, the simulations above may further over-estimate the cooling rate [44]. The effect of this on the ambient ECP temperature is shown in Figure 4.6 for the case of repeated ECP use. The result shows that the ECP is significantly cooler given the reduced solar data, the ECP will return to the ambient temperature at a similar time.

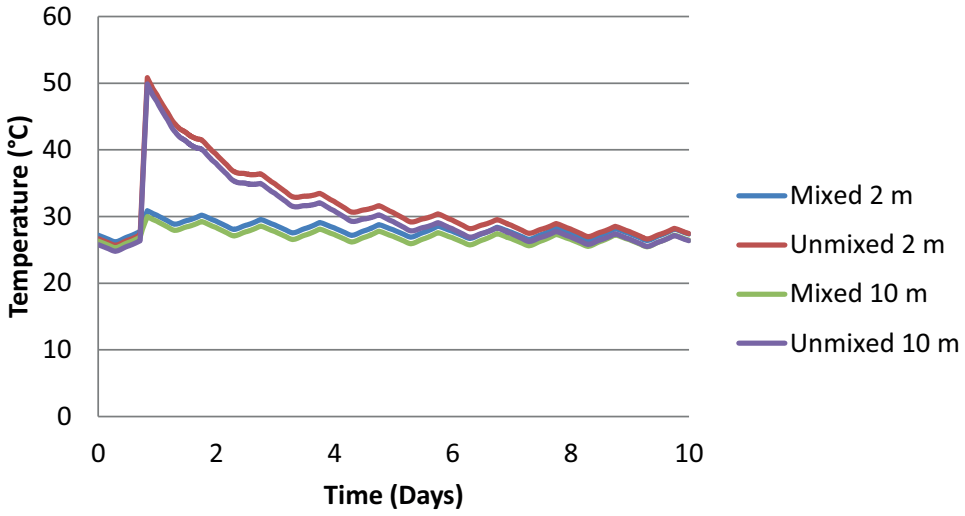

Figure 4.5: ECP cooling rate for an uncorrected wind speed

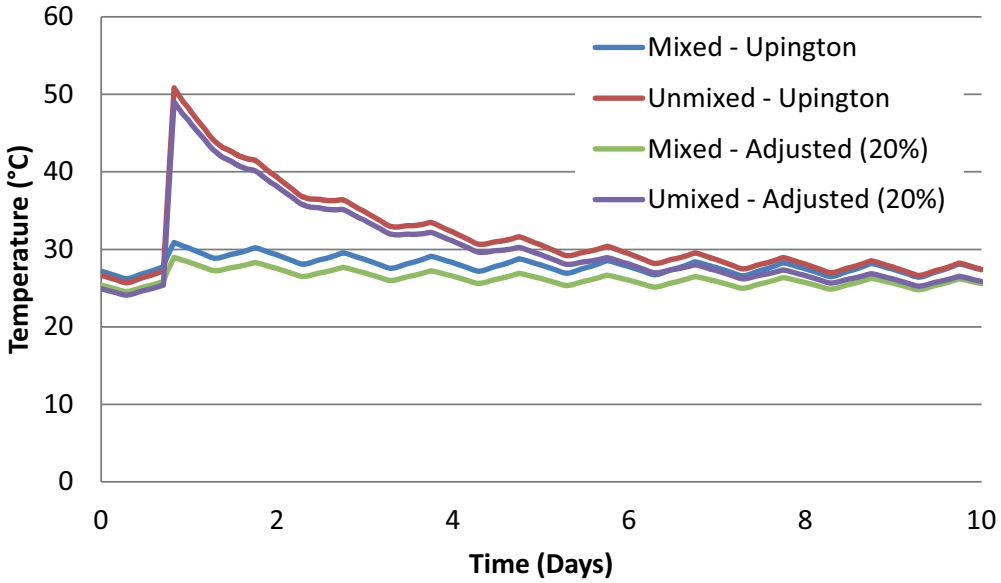

Figure 4.6: ECP cooling rate compared to a 20% reduction in solar heat addition

Finally the largest contributor, evaporation, is re-visited and a formal sensitivity study conducted. To do this the analytic derivative of the New-Ryan Equation with respect to various input parameters was constructed (Appendix D).The calculated expected error due to uncertainties in measured input data was then found to be no more than $0.5°C$.

From the above, the ECP is deemed a viable solution for the reduction in load losses at Matimba Power Station. The validated ECP model shows that although the pond is capable of sustainable operation under even severe conditions.

4.2 Mass Transfer Results

An important output for this study is the mass of water lost as a result of evaporation. The typical chemical profile provided in Table 1.1 is likely to be detrimental to the pipework and heat exchanger surfaces. The evaporation of water from the ECP will further increase the concentration of harsh chemicals in the water. Furthermore, the waste water supplied to the ECP is not going to dilute the ECP water as it will continue to add contaminants. While the design of the plant will consider these factors through the use of coatings and materials which can withstand the poor water quality, the water chemistry will need to be maintained within suitable operating conditions.

The quantity of water lost through evaporation on a daily basis is evaluated for the two primary cases. Firstly the single cycle ECP operation and secondly, operation over ten days. Directly following the addition of heat to the ECP, it is found that approximately 2000 l is lost as a result of evaporative mass transfer. This rate decreases as the ECP cools down.

Operation whereby the ECP experiences five heating cycles over a ten day period (see Figure 4.8), shows that the water lost through evaporative mass transfer increases to 2500 l/day. An estimated 5.5% of the water is lost during this period and water evaporates at a typical rate of $22kg/m^2$. The ECP will need between 2000 and 2500 litres of water daily to replenish water loss through evaporation. The change in the ECP chemical profile as a result of this evaporative mass transfer can be established and the relevant water treatment plants designed for operation.

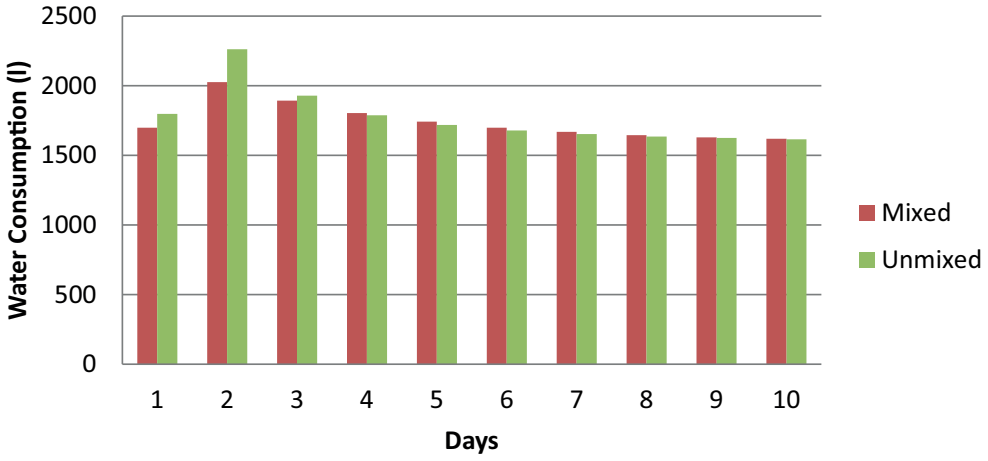

Figure 4.7: Daily water consumption after a single heating cycle

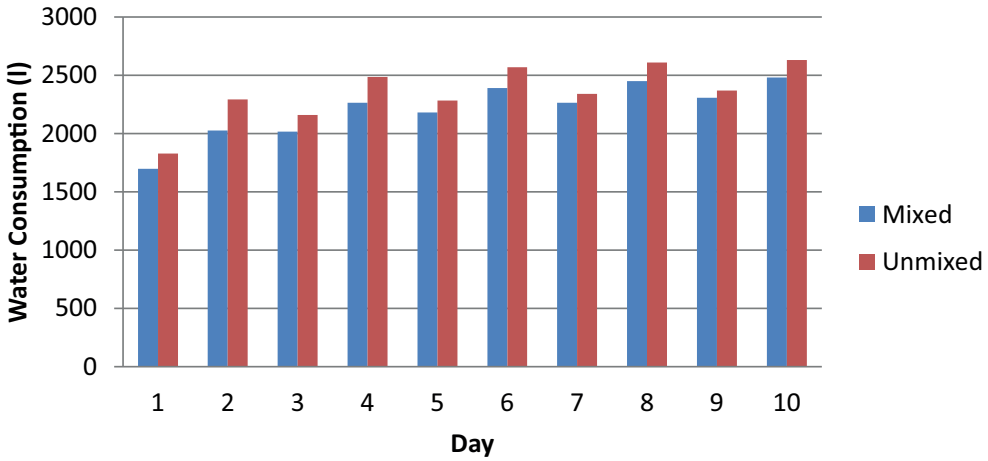

Figure 4.8: Daily consumption of water over 5 operating cycles

Chapter 5

Conclusions

The study is aimed at drastically reducing the Vacuum Load Losses experienced on a single unit at Matimba Power Station during adverse atmospheric conditions. The thermal load on the ACC is reduced by condensing a portion of the steam leaving the turbine exhaust. Cooling water supplying the surface condenser is pumped from an existing waste water pond and once heated it is returned to the pond where it would be left to cool.

A model that could be used to make critical design decisions is needed. While pond models have been developed in the past, none of those available in open literature could be used for the pond at Matimba. The pond is unique in that it has a large surface area to depth ratio. Further, from an analysis of the various modes of heat exchange effecting the pond, it was concluded that the most appropriate model would be a lumped thermal capacity model. For this model the modes of heat exchange to be considered are: evaporation, thermal convection, atmospheric radiation, solar radiation and ground conduction.

Evaporation is a primary driver for heat transfer in the ECP. Heat is transferred via the vaporisation of water at the pond surface, causing a loss of pond mass. Estimation of this phenomenon at the pond surface is complex. The environment is constantly changing and the scales influencing this pond requires consideration. In this study the correlations for evaporation found in literature rigorously evaluated. From this the New Ryan Equation was selected as most accurate for predicting evaporation. The correlation had been calibrated on a variety of pond surfaces and accounted for the the size of a pond. Convection is modelled using a correlation and developed

for applications where surfaces are exposed to the open environment. Atmospheric radiation is predicted using an experimentally tested correlation. Solar radiation is calculated using a procedure commonly used in the open literature using the input data available. Lastly, the pond base is lined and the only mode of heat exchange is via ground conduction. For such conditions a numerical solution to the one dimensional heat conduction equation is developed with appropriate boundary conditions found in literature.

The various heat exchange modes were applied to a computer model using C++, the model is designed to be modular allowing for various correlations to be tested. This has the potential for application in further studies using modern numerical tools. The model is validated using experimental data from tests conducted in an area with atmospheric conditions similar to that at Matimba. Using data from the four experiments, conducted on a pond with a surface area of 3 $600m^2$, the model developed in this study was found to accurately predict the pond temperature (within 5%). The sensitivity of the model to various input parameters were tested, in these tests it was found that the model would deviate within acceptable bounds.

Assuming that the pond is to supply water at ambient temperatures it is found that the ECP can sustainably support even extreme conditions. This includes using the ECP to augment cooling for three hours per day every second day, during the hottest months. This would result in cooling water of temperature range of $27°C$ and $31°C$ after ten days of operation.

Water loss as a result of evaporation is calculated in this model. It was found that between 2000 and 2500 litres of water is lost per day through evaporative mass transfer during operation. This information can be used to design plant which would regulated the chemical composition of water in the pond. The study found that during ten days of operation, 5.5% of the pond volume is lost through evaporative mass transfer.

To conclude, the study has shown that the ECP at Matimba Power Station is a viable source of additional cooling for the plant. The mathematical model developed shows that it would be practical to operate the pond intermittently and have a reliable source of cold water for the condenser. Using the model developed, the size of the components which make up the ECP can be quantified. The potential to further improve this model exists through the use of modern numerical tools, such as CFD, to predict the effect of internal flows within the pond, and improve the correlations for heat exchange at the surface.

Bibliography

[1] D. G. Kröger. *Air Cooled Heat Exchangers and Coolling Towers*. University of Stellenbosch, 1998.

[2] H. B. Goldschagg. *Utilising Matimba's Evaporation Ponds to Eliminate Vacuum Losses on Unit 1*. Eskom Holdings SOC, November 2011.

[3] Adams E.E., Cosler D.J., and Helfrich K.R. Analysis of evaporation data from heated ponds. Technical report, EPRI, 1987.

[4] Adams E. E., Helfrich K. R., Godbey A. L., and Harleman D. R. F. Evaluation of models for predicting evaporative water loss in cooling impoundments. Technical report, EPRI, 1982.

[5] G. R. Branfield. Thermal characteristics of a greenhouse for aquaculture. Master's thesis, University of Stellenbosch. Faculty of Engineering. Dept. of Mechanical and Mechatronic Engineering., 2006.

[6] C.F. Cerco. Experimental and analytic study of the design of cooling ponds. Master's thesis, Massachusetts Institute of Technology, 1977.

[7] G.F. Athey, R.K. Hadlock, O.B. Abbey, Pacific Northwest Laboratory, Siting U.S. Nuclear Regulatory Commission. Division of Health, and Waste Management. *Ultimate Heat Sink Thermal Performance and Water Utilization: Measurements on Cooling and Spray Ponds*. The Commission, 1982.

[8] A. F. du Preez and J. P. Pretorius. Discussion with Eskom personnel, 2013.

[9] F. G. Louw. *Performance Trends of a Large Air-Cooled Steam Condenser during Windy Conditions*. PhD thesis, University of Stellenbosch, 2011.

[10] H. B. Goldschagg. Lessons learned from the world's largest forced draft-direct air-cooled condenser. In *EPRI International Symposium on Improved Technology for Fossil Power Plants- New and Retrofit applications*, 1993.

[11] J. Imberger and P. F. Hamblin. Dynamics of lakes, resevoirs and cooling ponds. *Annual Review of Fluid Mechanics*, 14:153–187, 1982.

[12] G. Kirillin. *Modeling of the Vertical Heat Exchange in Shallow Lakes*. PhD thesis, Humboldt-Universität zu Berlin, 2002.

[13] C. Angeli, E. Leonardi, and L. Maciocco. A computational study of salt diffusion and heat extraction in solar pond plants. *Solar Energy*, 80(11):1498 – 1508, 2006.

[14] G.H. Jirka and D. R. F. Harleman. Cooling impoundments: Classification and analysis. *Journal of the Energy Division*, 105:291–309, 1979.

[15] Jerome M Raphael. Prediction of temperature in rivers and reservoirs. *Journal of the Power Division, Vol 88, No P 02, July, 1962, P 157.*, 1962.

[16] H. E. Jobson. The dissipation of excess heat from water systems. *Journal of the Power Division*, 99:89–103, 1973.

[17] I.A. Olwi, J.A. Sabbagh, and A.M.A. Khalifa. Mathematical modeling of passive dry cooling for power plants in arid land. *Solar Energy*, 48(5):279 – 286, 1992.

[18] A. D. Chiasson. Advances in modeling of ground-source heat pump systems. Master's thesis, Oklahoma State University, 2000.

[19] H. Rubin, B. A. Benedict, and S. Bachu. Modeling the performance of a solar pond as a source of thermal energy. *Solar Energy*, 32:771–778, 1984.

[20] E. L. Peterson, J. A. Harris, and L. C. Wadhwa. CFD modelling pond dynamic processes. *Aquacultural Engineering*, 23(13):61 – 93, 2000.

[21] R. Codell, W.K. Nuttle, and U.S. Nuclear Regulatory Commission. Office of Nuclear Reactor Regulation. Division of Engineering. *Analysis of Ultimate Heat Sink Cooling Ponds*. Number v. 88 in Analysis of Ultimate Heat Sink Cooling Ponds. Division of Engineering, Office of Nuclear Reactor Regulation, U.S. Nuclear Regulatory Commission, 1980.

[22] F.P. Incropera, P. P. Dewitt, T.L. Bergman, and A. S. Lavine. *Fundamentals of Heat and Mass Trasfer*. John Wiley and Sons, 2007.

[23] E. Sartori. A critical review on equations emloyed for the calculation of the evapration rate from free water. *Solar Energy*, 68:77–89, 2000.

[24] M.M. Gonzalez-Real A. Baille J.M. Molina Martinez, V. Martinez Alvarez. A simulation model for predicting hourly pan evaporation from meteorological data. *Journal of Hydrology*, 318:250–261, 2006.

[25] J. Dalton. *Experimental Essays*. Memoirs of the Lit & Phil, 1802.

[26] T. P. Yilmaz and H. S. Aybar. Evaluation of the correlations for predicting evaporative loss from water body. In *ASHRAE Proceedings*, 1999.

[27] K. D. Brady, W. L. Geyer, and J. C. Graves. Cooling water studies for edison electric institute. Technical Report RP-49 Surface Heat Exchange at Power Plant Cooling Lakes, Johns Hopkins University, 1969.

[28] P.J. Ryan and D.R.F. Harleman. *An analytical and experimental study of transient cooling pond behavior*. Report (Ralph M. Parsons Laboratory for Water Resources and Hydrodynamics). Dept. of Civil Engineering, Massachusetts Institute of Technology, 1973.

[29] D.T. Bailey. *Meteorological monitoring guidance for regulatory modeling applications*. U.S. Environmental Protection Agency, Office of Air and Radiation, Office of Air Quality Planning and Standards, 2000.

[30] W. Brutsaert and G. Yeh. Implications of a type of empirical evaporation formula for lakes and pans. *Water Resources Research*, 6(4):1202–1208, 1970.

[31] I. T. Webster and B.S. Sherman. Evaporation from fetch-limited water bodies. *Irrigation Science*, 16:53–64, 1995.

[32] S.A Condie and I. T. Webster. The influence of wind stress, temperature, and humidity gradients on evaporation from reservoirs. *Water Resources Research*, 33(12):2813–2822, December 1997.

[33] G. E. Harbeck. A practical field technique for measuring reservoir evaporation utilising mass-transfer theory. *Geological Survey Professional*, 62:101–105, 1962.

[34] D.L. McJannet, I. T. Webster, and F.J. Cook. An area-dependent wind function for estimating open water evaporation using land-based meteorological data. *Environmental Modelling and Software*, 31:76–83, 2012.

[35] D. G. Kröger. Convection heat transfer between a horizontal surface and the natural environment. *R&D Journal*, 18:49–54, 2002.

[36] A. L. Buck. New equations for computing vapor pressure and enhancement factor. *Journal of Applied Meteorology*, 20(12):1527–1532, 1981.

[37] M. Burger. Prediction of the temperature distribution in asphalt pavement samples. Master's thesis, University of Stellenbosch, 2005.

[38] E. Sartori. Convection coefficient equations for forced air flow over flat surfaces. *Solar Energy*, 80(9):1063 – 1071, 2006.

[39] J. P. Pretorius. *Optimization and Control of a Large-scale Solar Chimney Power Plant*. PhD thesis, University of Stellenbosch, 2007.

[40] P Berdahl and R Fromberg. The thermal radiance of clear skies. *Solar Energy*, 29(4):299 – 314, 1982.

[41] J. A. Duffie and W. A. Beckman. *Solar engineering of thermal processes*. Wiley New York, 2nd ed. edition, 1991.

[42] R. A. Hedderwick. Performance evaluation of a solar chimney power plant. Master's thesis, University of Stellenbosch, 2000.

[43] Eskom RT&D. Solar radiation measurements: Upington 2007.

[44] Solar radiation maps. http://solargis.info. Accessed: 2013-12-11.

Appendix A

Sample Calculation

The input data for the sample calculation is given in Table A.1. From this information the evaporation, convection and atmospheric radiation calculations are shown below. Items marked with a * denotes fluid property data taken from equations in Appendix B.

The vapour pressure is calculated using Equation (B.5)

$$P_{vs}(313.15) = 7377 \tag{A.1}$$

$$P_{v\infty}(298.15) = 3166Pa \tag{A.2}$$

$$\begin{aligned} T_{ave} &= \frac{T_s+T_\infty}{2} \\ &= \frac{298.15+313.15}{2} \\ &= 305.65K \end{aligned} \tag{A.3}$$

$$\begin{aligned} e_s &= \Phi_{rh_s} P_{vs} \\ &= (1)(7377) \\ &= 7377Pa \end{aligned} \tag{A.4}$$

Table A.1: Sample Calculation Input Data

Variable	**Symbol**	**Value**
Dry Bulb Temperature	T_∞	$25°C = 298.15K$
Pond Surface Temperature	T_s	$40°C = 313.15K$
Relative Humidity	Φ_{rh}	0.44
Wind Speed	v_w	$3\frac{m}{s}$
Air Pressure	Pa	$101325Pa$
Dew Point Temperature	T_{dp}	$284.244K$
Surface Area	A	$3600m^2$
Viscosity	μ	$1.88 \times 10^{-5} \frac{kg}{sm}$
Specific Heat[1]	c_p	$1007.24\frac{J}{kgK}$
Thermal Conductivity[1]	k	$0.0267804\frac{W}{mK}$
Density[1]	ρ	$1.13\frac{kg}{m^3}$
Gravitational Acceleration	g	$9.81\frac{m}{s^2}$
Emissivity Water [18]	ϵ	0.9

$$\begin{aligned} e_\infty &= \Phi_{rh_\infty} P_{v\infty} \\ &= (0.45)(3166) \\ &= 1393.36Pa \end{aligned} \tag{A.5}$$

$$\begin{aligned} \theta_{vs} &= \frac{T_s}{1-\frac{0.378e_s}{Pa}} \\ &= \frac{313.15}{1-\frac{0.378(7377)}{101325}} \\ &= 322.01K \end{aligned} \tag{A.6}$$

$$\begin{aligned} \theta_\infty &= \frac{T_\infty}{1-\frac{0.378e_\infty}{P_a}} \\ &= \frac{298.15}{1-\frac{(0.378)(1393)}{101325}} \\ &= 299.708K \end{aligned} \tag{A.7}$$

$$\begin{aligned} \Delta\theta_v &= \theta_{vs} - \theta_\infty \\ &= 321.98 - 301.71 \\ &= 22.3 \end{aligned} \tag{A.8}$$

$$\begin{aligned} q_{evap} &= \sqrt{(2.7\Delta\theta_v^{\frac{1}{3}})^2 + (5.1A^{-0.05}v)^2 \frac{e_s - e_\infty}{100}} \\ &= \sqrt{(2.7(20.27)^{\frac{1}{3}})^2 + (5.1\frac{3600}{10000}^{-0.05}(3))^2 \frac{7354-3162}{100}} \\ &= 1065.16\frac{W}{m^2} \end{aligned} \tag{A.9}$$

$$\begin{aligned} q_{conv} &= \left(0.2106\left(\frac{\mu T}{g(T_o - T_i)c_p k^2 \rho^2}\right)^{\frac{1}{3}} + v_w \left(\frac{0.0052}{2}\right)\left(\frac{c_p k^2 \rho^3}{\mu^2}\right)^{\frac{1}{3}}\right)(T_s - T_\infty) \\ &= \left(0.2106\left(\frac{(0.000118)305.65}{9.81(313.15-298.15)(1007.24)(0.026)^2(1.13)^2}\right)^{\frac{1}{3}} + 3\left(\frac{0.0052}{2}\right)\left(\frac{(1007.24)(0.026)(1.13)^3}{0.00018^2}\right)^{\frac{1}{3}}\right) \\ &\times (313.15 - 298.15) \\ &= 265.5\frac{W}{m^2} \end{aligned} \tag{A.10}$$

$$\begin{aligned} \epsilon_{sky} &= 0.741 + 0.0062T_{dp} \\ &= 0.741 + 0.0062(284.244) \\ &= 2.50 \end{aligned} \tag{A.11}$$

$$\begin{aligned} q_{rad} &= \epsilon_w \sigma \left(T_s^4 - \epsilon_{sky} T_a^4\right) \\ &= (0.9)(0.00000005670373)\left(313.15^4 - 2.5(298.15)^4\right) \\ &= 62.75\frac{W}{m^2} \end{aligned} \tag{A.12}$$

Appendix B

Fluid Property Data

This chapter provides all correlations used to estimate fluid properties in this thesis. For these equations all temperatures (T) should be in K.

B.1 Air Properties [1]

Density:

$$\rho_{air} = \frac{P_a}{287.08T} \tag{B.1}$$

Specific Heat:

$$\begin{aligned} c_{pair} &= 1.045356 \times 10^3 - 3.161783 \times 10^{-1}T \\ &+ 7.083814 \times 10^{-4}T^2 - 2.705209 \times 10^{-7}T^3 \end{aligned} \tag{B.2}$$

Dynamic Viscosity:

$$\begin{aligned} \mu_{air} &= 2.287973 \times 10^{-6} + 6.259793 \times 10^{-8}T \\ &- 3.131956 \times 10^{-11}T^2 + 8.15038 \times 10^{-15}T^3 \end{aligned} \tag{B.3}$$

Thermal Conductivity:

$$\begin{aligned} k_{air} &= -4.937787 \times 10^{-4} + 1.018087 \times 10^{-4} T \\ &- 4.627937 \times 10^{-8} T^2 + 1.250603 \times 10^{-11} T^3 \end{aligned} \tag{B.4}$$

B.2 Saturated Vapour Properties [1]

Thermophysical properties of saturated water vapour from $273.15K$ to $380K$

$$\begin{aligned} P_v &= 10^z \\ z &= 10.79586\,(1 - 273.16/T) + 5.02808 log_{10}\,(273.16/T) \\ &+ 1.50474 \times 10^{-4}\left(1 - 10^{-8.29692((T/273.16)-1)}\right) \\ &+ 4.2873 \times 10^{-4}\left(10^{4.76955(1-273.16/T)}\right) \end{aligned} \tag{B.5}$$

Specific Heat:

$$\begin{aligned} c_{pv} &= 1.3605 \times 10^3 + 2.31334 T - 2.46784 \times 10^{-10} T^5 \\ &+ 5.91332 \times 10^{-13} T^6 \end{aligned} \tag{B.6}$$

Dynamic Viscosity:

$$\begin{aligned} \mu_v &= 2.562435 \times 10^{-6} + 1.816683 \times 10^{-8} T \\ &+ 2.579066 \times 10^{-11} T^2 - 1.067299 \times 10^{-14} T^3 \end{aligned} \tag{B.7}$$

Thermal Conductivity:

$$\begin{aligned} k_v &= 1.3046 \times 10^{-2} - 3.756191 \times 10^{-5} T \\ &+ 2.217964 \times 10^{-7} T^2 - 1.111562 \times 10^{-10} T^3 \end{aligned} \tag{B.8}$$

Density:

$$\begin{aligned}\rho_v &= -4.062329056 + 0.10277044T - 9.76300388 \times 10^{-4}T^2 \\ &+ 4.475240795 \times 10^{-6}T^3 - 1.004596894 \times 10^{-8}T^4 \\ &+ 8.9154895 \times 10^{-12}T^5\end{aligned} \tag{B.9}$$

$$\begin{aligned}T_v &= 164.630366 + 1.832295 \times 10^{-3}P_v + 4.27215 \times 10^{-10}P_v^2 \\ &+ 3.738954 \times 10^3 P_v^{-1} - 7.01204 \times 10^5 P_v^{-2} \\ &+ 16.161488ln\left(P_v\right)1.437169 \times 10^{-4}P_v in\left(P_v\right)\end{aligned} \tag{B.10}$$

B.3 Air and Water Vapour [1]

Density:

$$\overline{\rho}_{av} = \left(1+\omega\right)\left(1-\omega\left(\omega+0.62198\right)\right)P_{abs}/(287.08T) \tag{B.11}$$

Specific Heat:

$$\overline{c_{pav}} = \left(c_{pair} + \omega c_{pv}\right)\left(1+\omega\right) \tag{B.12}$$

$$\overline{c_{pma}} = \left(c_{pair} + \omega c_{pv}\right) \tag{B.13}$$

Dynamic Viscosity

$$\overline{\mu_{av}} = \frac{X_a \mu_a M_a^{0.5} + X_v \mu_v M_v^{0.5}}{X_a M_a^{0.5} + X_v M_v^{0.5}} \tag{B.14}$$

Where $M_a = 28.97kg/mole$, $M_v = 18.016kg/mole$, $X_a = 1/(1+1.608\omega)$ and $X_v = \omega/(\omega+0.622)$

Thermal Conductivity

$$\overline{\mu_{av}} = \frac{X_a k_a M_a^{0.33} + X_v k_v M_v^{0.33}}{X_a M_a^{0.33} + X_v M_v^{0.33}} \tag{B.15}$$

Humidity Ratio:

$$\begin{aligned} \omega &= \left(\frac{2501.6 - 2.3263(T_{wb} - 273.15)}{2501.6 + 1.8577(T - 273.15) - 4.184(T_{wb} - 273.15)}\right)\left(\frac{0.62509 P_{vwb}}{P_{abs} - 1.005 P_{vwb}}\right) \\ &- \left(\frac{1.00416(T - T_{wb})}{2501.6 + 1.8577(T - 273.15) - 4.184(T_{wb} - 273.15)}\right) \end{aligned} \tag{B.16}$$

B.4 Water Liquid [1]

These properties are valid for the temperature range 273.15K to 380K.

$$\begin{aligned} \rho_{water} &= (1.49343 \times 10^{-3} - 3.7164 \times 10^{-6} T + 7.09782 \times 10^{-9} T^2 \\ &- 1.90321 \times 10^{-20} T^6)^{-1} \end{aligned} \tag{B.17}$$

$$\begin{aligned} c_{pwater} &= 8.15599 \times 10^3 - 28.0627 T + 5.11283 \times 10^{-2} T^2 \\ &- 2.17582 \times 10^{-13} T^6 \end{aligned} \tag{B.18}$$

$$\mu_{water} = 2.414 \times 10^{-5} \times 10^{247.8/(T - 140)} \tag{B.19}$$

$$\begin{aligned} k_{water} &= -6.14255 \times 10^{-1} + 6.9962 \times 10^{-3} T - 1.01075 \times 10^{-5} T^2 \\ &+ 4.74737 \times 10^{-12} T^4 \end{aligned} \tag{B.20}$$

Appendix C

Experimental Data and Analysis

C.1 Experimental Data

The experimental data for the tests conducted at East Mesa can be found in the Appendix of the publication by Hadlock et.al. [7]. For this study the data presented are from Experiment 3 and 4 of these tests, for completeness the primary input data are provided below.

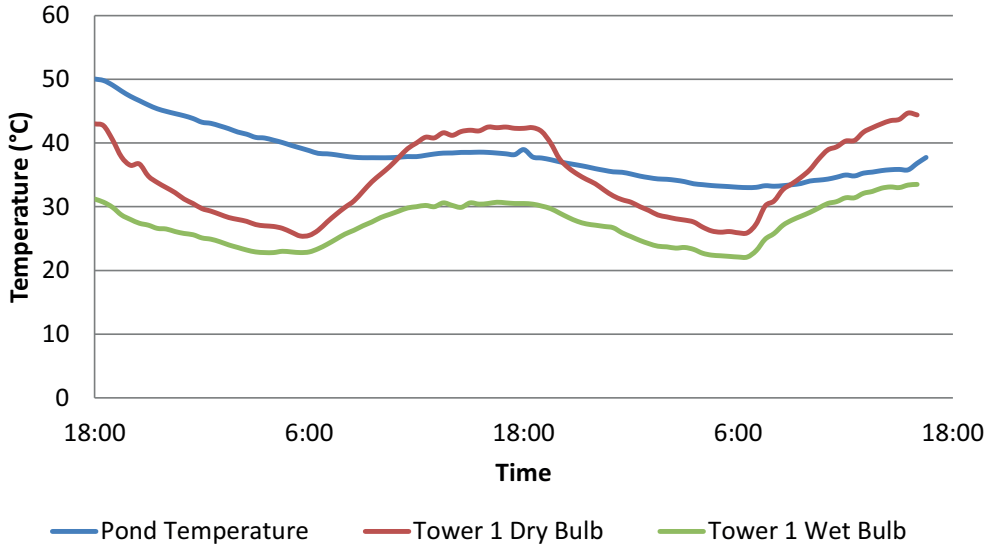

Figure C.1: Temperature Readings at East Mesa Experiment 3

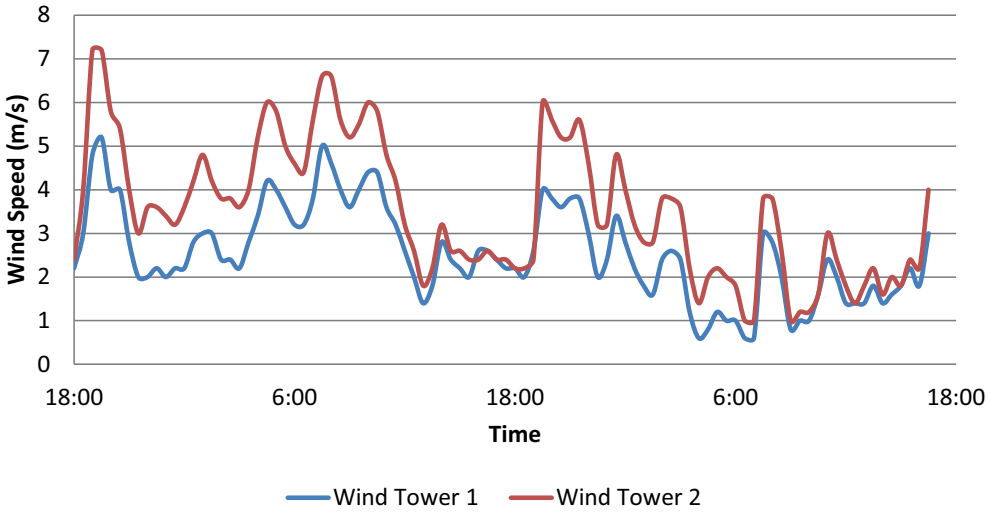

Figure C.2: Wind Speed Readings at East Mesa Experiment 3

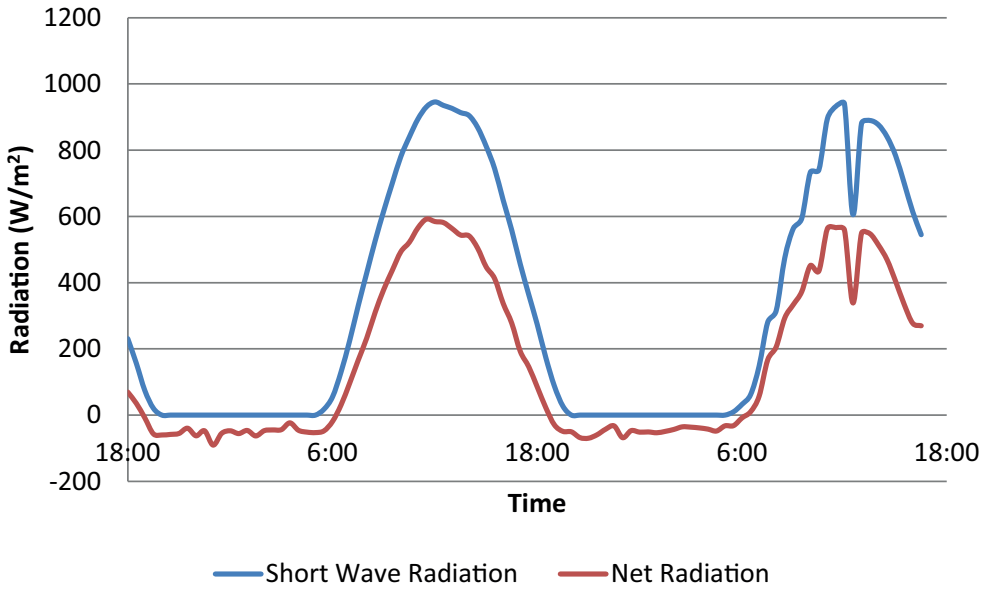

Figure C.3: Radiation Readings at East Mesa Experiment 3

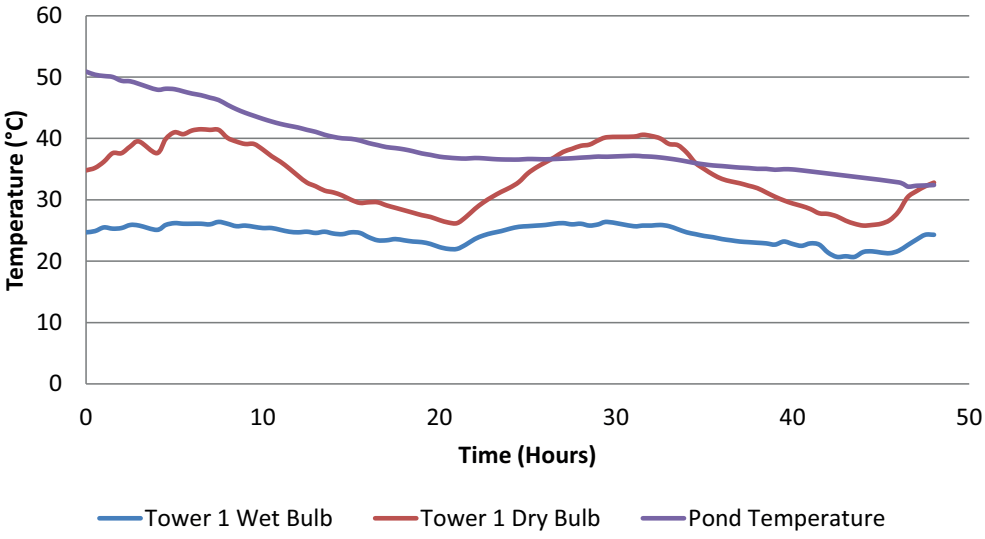

Figure C.4: Temperature Readings at East Mesa Experiment 4

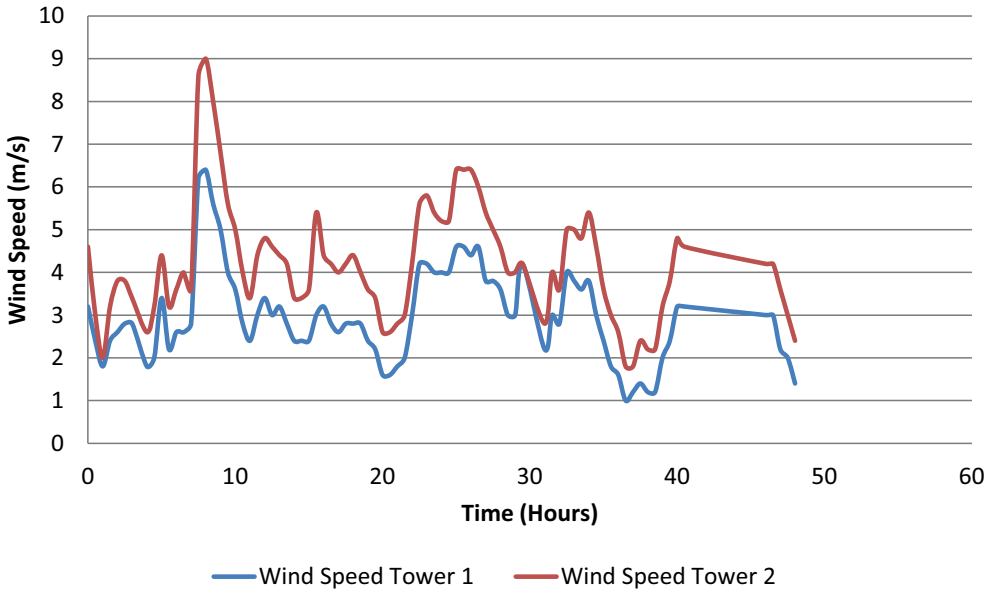

Figure C.5: Wind Speed Readings at East Mesa Experiment 4

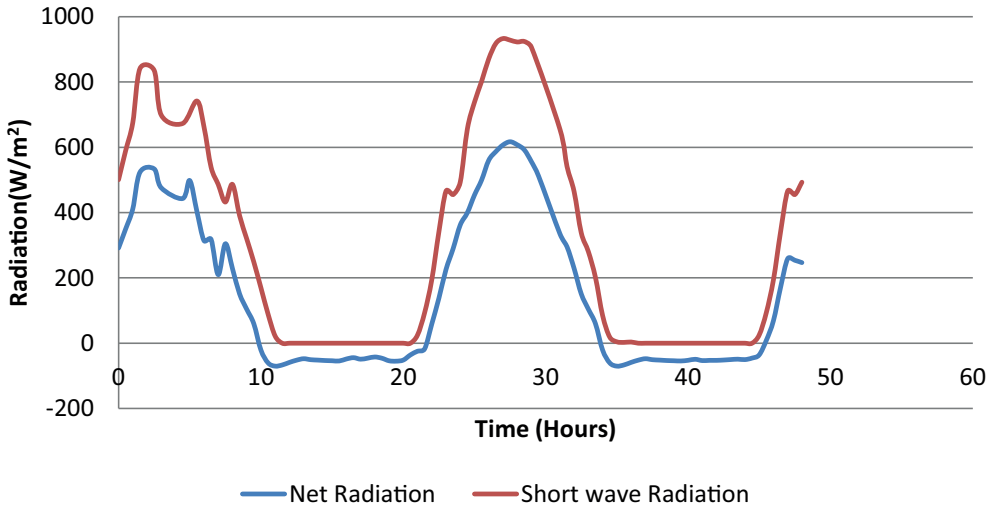

Figure C.6: Radiation Readings at East Mesa Experiment 4

Appendix D

Sensitivity Analysis

In order to do a sensitivity analysis of the variables that affect these correlations the following partial derivatives were taken.

$$q_{evap} = \left(2.7\Delta\theta_v^{\frac{1}{3}} + 3.1W_2\right)(e_s - e_a) \tag{D.1}$$

$$\frac{\partial q_{evap}}{\partial W_2} = 3.1\,(e_s - e_a) \tag{D.2}$$

$$q_{evap} = \left(2.7\,(\theta_s - \theta_a)^{\frac{1}{3}} + 3.1W_2\right)(e_s - e_a) \tag{D.3}$$

$$\frac{\partial q_{evap}}{\partial T_s} = \left(\frac{2.7}{3}\,(\theta_s - \theta_a)^{-\frac{2}{3}}\,\frac{\partial \theta_s}{\partial T_s}\right)(e_s - e_a) + \left(2.7\,(\theta_s - \theta_a)^{\frac{1}{3}} + 3.1W_2\right)\frac{\partial e_s}{\partial T_s} \tag{D.4}$$

$$\frac{\partial e_s}{\partial T_s} = -\frac{\alpha\beta}{T_s^2}e^{\frac{\beta}{T_s}} \tag{D.5}$$

$$\frac{\partial \theta_s}{\partial T_s} = \frac{\left(1 - \frac{0.378 e_s}{P_a}\right) + \left(T_s \frac{0.378 \frac{\partial e_s}{\partial T_s}}{Pa}\right)}{\left(1 - \frac{0.378 e_s}{P_a}\right)^2} \tag{D.6}$$

$$\frac{\partial q_{evap}}{\partial T_a} = \left(-\frac{2.7}{3}\left(\theta_s - \theta_a\right)^{-\frac{2}{3}} \frac{\partial \theta_a}{\partial T_a}\right)\left(e_s - e_a\right) + \left(2.7\left(\theta_s - \theta_a\right)^{\frac{1}{3}} + 3.1 W_2\right)\left(-\frac{\partial e_a}{\partial T_a}\right) \tag{D.7}$$

$$\frac{\partial e_a}{\partial T_a} = -\frac{\phi \alpha \beta}{T_a^2} e^{\frac{\beta}{T_a}} \tag{D.8}$$

$$\frac{\partial \theta_a}{\partial T_a} = \frac{\left(1 - \frac{0.378 e_a}{P_a}\right) + \left(T_a \frac{0.378 \frac{\partial e_a}{\partial T_a}}{Pa}\right)}{\left(1 - \frac{0.378 e_a}{P_a}\right)^2} \tag{D.9}$$

$$\frac{\partial q_{evap}}{\partial \phi} = \left(-\frac{2.7}{3}\left(\theta_s - \theta_a\right)^{-\frac{2}{3}} \frac{\partial \theta_a}{\partial \phi}\right)\left(e_s - e_a\right) + \left(2.7\left(\theta_s - \theta_a\right)^{\frac{1}{3}} + 3.1 W_2\right)\left(-\frac{\partial e_a}{\partial \phi}\right) \tag{D.10}$$

$$\frac{\partial e_a}{\partial T_a} = \alpha e^{\frac{\beta}{T_a}} \tag{D.11}$$

$$\frac{\partial \theta_a}{\partial \phi} = \frac{\left(T_a \frac{0.378 \frac{\partial e_a}{\partial \phi}}{Pa}\right)}{\left(1 - \frac{0.378 e_a}{P_a}\right)^2} \tag{D.12}$$

$$e_s = \alpha e^{\frac{\beta}{T_s}} \tag{D.13}$$

$$e_a = \alpha \phi e^{\frac{\beta}{T_a}} \tag{D.14}$$

$$\theta_s = \frac{T_s}{1 - \frac{0.378\alpha e^{\frac{\beta}{T_s}}}{P_a}} \tag{D.15}$$

$$\theta_a = \frac{T_s}{1 - \frac{0.378\phi\alpha e^{\frac{\beta}{T_a}}}{P_a}} \tag{D.16}$$

$$q_{evap} = \left(2.7 \left(\frac{T_s}{1 - \frac{0.378\alpha e^{\frac{\beta}{T_s}}}{P_a}} - \frac{T_s}{1 - \frac{0.378\phi\alpha e^{\frac{\beta}{T_a}}}{P_a}} \right)^{\frac{1}{3}} + 3.1W_2 \right) \left(\alpha e^{\frac{\beta}{T_s}} - \alpha\phi e^{\frac{\beta}{T_a}} \right) \tag{D.17}$$